

A Universal Approach to Coverage Probability and Throughput Analysis for Cellular Networks

Hui Zhang, Sheng Chen, *Fellow, IEEE*, Liang Feng, Yifeng Xie, and Lajos Hanzo, *Fellow, IEEE*

Abstract—This paper proposes a novel tractable approach for accurately analyzing both the coverage probability and the achievable throughput of cellular networks. Specifically, we derive a new procedure referred to as the equivalent uniform-density plane-entity (EUDPE) method for evaluating the other-cell interference. Furthermore, we demonstrate that our EUDPE method provides a universal and effective means to carry out the lower bound analysis of both the coverage probability and the average throughput for various base-station distribution models that can be found in practice, including the stochastic Poisson point process (PPP) model, a uniformly and randomly distributed model, and a deterministic grid-based model. The lower bounds of coverage probability and average throughput calculated by our proposed method agree with the simulated coverage probability and average throughput results and those obtained by the existing PPP-based analysis, if not better. Moreover, based on our new definition of cell edge boundary, we show that the cellular topology with randomly distributed base stations (BSs) only tends toward the Voronoi tessellation when the path-loss exponent is sufficiently high, which reveals the limitation of this popular network topology.

Index Terms—Achievable throughput, cellular coverage, cellular networks, deterministic grid-based model, Poisson point process (PPP) model, uniformly and randomly distributed model.

I. INTRODUCTION

SINCE cellular systems are under growing pressure to increase the volume of data delivered to consumers, establishing an accurate performance prediction model is of prime significance [1]. Cellular systems are evolving into a large-scale heterogeneous network architecture, constructed by overlapping network tiers, such as macrocells, picocells, femtocells, etc. [2]–[4]. The traditional cellular analysis relying on an idealized hexagonal model does not realistically represent the actual distribution of cells. Clearly, such a simplistic model

cannot be used for accurately modeling real-world cellular networks and for analyzing the coverage probability and the achievable throughput. Two mathematical models, i.e., the cellular system interference model and the base station (BS) or cell distribution model, are fundamental in the coverage analysis.

A. Related Work and Motivation

According to [5], the interference models can generally be divided into two types: empirical models and statistical–physical models. The construction of an empirical interference model relies on first measuring the interference and then fitting a mathematical model to the data. By contrast, the derivation of a statistical–physical model usually relies on the mathematical modeling of the interference. The classic Wyner model [6] was proposed in 1994, and since then, it has been widely adopted in the analysis of cellular networks. This model assumes that the interference is constituted by the sum of the signals transmitted from the adjacent cells (typically only considering two neighbors), which is often multiplied by a fixed scaling factor or gain to represent the specific intensity of the interferers [6]–[9].

Determining the most beneficial positions of the BSs represents a critical planning problem in cellular networks. Traditional methods usually place the BSs deterministically on a regular grid, despite the fact that, in practice, the positions of BSs are influenced by many random factors. Taking into account the randomness of BS locations, in [10] and [11], a stochastic-geometry-based method for modeling the positions of the BSs was derived, whereas in [12] and [13], it was proposed that the BSs be placed according to a homogeneous Poisson point process (PPP) associated with a given intensity [12], [13]. However, since the cellular network is gradually evolving into a large-scale heterogeneous network associated with multiple-tier random BS locations, the design challenge becomes more grave. A recent contribution [14] has demonstrated that the BS locations may be drawn from a PPP, particularly for single-tier networks. In [5], the statistical–physical modeling of cochannel interference (CCI) was investigated by assuming that the geographic distribution of interferers is known *a priori* and that the interferers belong to a Poisson field, with each individual interferer having a random session life time. In [15], a mathematical theory based on a spatially homogeneous PPP was provided to analyze the effects of interference, which models the spatial distribution of the nodes over the 2-D infinite plane by PPP theory.

The PPP model was used in [12] for establishing a heterogeneous network model of a single-tier macrocell network.

Manuscript received March 5, 2014; revised August 31, 2014; accepted October 28, 2014. This work was supported in part by the National Natural Science Foundation Project of China under Grant 61101084 and in part by the Fundamental Research Funds for the Central Universities, China. The review of this paper was coordinated by Dr. Y. Ma.

H. Zhang, L. Feng, and Y. Xie are with the Wireless Communications Laboratory, Information College, Nankai University, Tianjin 300071, China (e-mail: zhangh@nankai.edu.cn; fengliang201203@gmail.com; xyfhope@gmail.com).

S. Chen is with the School of Electronics and Computer Science, University of Southampton, Southampton SO17 1BJ, U.K., and also with King Abdulaziz University, Jeddah 21589, Saudi Arabia (e-mail: sqc@ecs.soton.ac.uk).

L. Hanzo is with School of Electronics and Computer Science, University of Southampton, Southampton SO17 1BJ, U.K. (e-mail: lh@ecs.soton.ac.uk).

Color versions of one or more of the figures in this paper are available online at <http://ieeexplore.ieee.org>.

Digital Object Identifier 10.1109/TVT.2014.2366597

84 Based on this PPP model, the calculation of the cumulative
 85 interference imposed by all surrounding BSs can be carried
 86 out with the aid of the Laplace transform and the probability
 87 generating function [12], [14]. Furthermore, the coverage prob-
 88 ability expression was deduced for the specific scenario, when
 89 the interference experiences Rayleigh fading, and the results
 90 of [12] and [14] demonstrated that the analysis based on the
 91 PPP-aided modeling represent the lower bound of simulation
 92 results.¹ Similarly, the achievable average rate was also calcu-
 93 lated. Although the PPP model is adopted for the analysis of
 94 cellular networks, it is only accurate for sparse networks. By
 95 contrast, it suffers from a lack of realism in the case of dense
 96 networks since it may place several BSs far too closely together,
 97 which does not make practical sense as such a situation will not
 98 occur in a real BS deployment. It may impose excessive CCI if
 99 too many BSs are deployed too densely. Noting this weakness
 100 of the PPP model, some balanced measures are suggested to
 101 alleviate this drawback in [12], but this weakness cannot be fun-
 102 damentally eliminated by these measures. Moreover, the PPP-
 103 based analysis relies on the assumption that the transmitters are
 104 independently distributed [16].

105 A range of alternative stochastic-geometry-based methods
 106 have also been used in the analysis of wireless networks [17],
 107 [18]. For example, in [17], the Matérn hard-core process was
 108 invoked for modeling the classic carrier sense multiple access
 109 (CSMA) protocol and for analyzing its throughput, where the
 110 presence of interferers within a given radius around any trans-
 111 mitter was prevented. The Matérn point process [19] was modi-
 112 fied in [18] to model the CSMA with collision avoidance, which
 113 yields more realistic results by applying the aforementioned
 114 interference-exclusion zone around all possible transmitters.
 115 However, coverage analysis based on a Matérn hard-core pro-
 116 cess is difficult to carry out [20] since the probability generating
 117 functional of a Matérn hard-core process does not exist. It was
 118 argued in [20]–[22] that only the Matérn type II process causes
 119 a level of interference comparable to that predicted by a PPP
 120 and, therefore, for interference-based performance analysis, the
 121 Matérn type II process may be safely approximated by the
 122 corresponding nonhomogeneous PPP [20]–[22].

123 B. Our Approach and Contributions

124 Against the above background, we propose a novel universal
 125 approach for tractable and accurate coverage analysis of cellu-
 126 lar networks. Our contributions are as follows.

127 1) *Physical Analysis of Hexagonal/Voronoi Cells:* To inter-
 128 pret the various geometric-based cellular models from a physi-
 129 cal perspective, we provide a tangible generic definition of the
 130 cell edge boundary for our theoretical analysis, where the cell
 131 boundary is directly linked to the path-loss exponent. Specif-
 132 ically, we show that the traditional hexagonal topology natu-
 133 rally emerges from the grid-based model, given a sufficiently
 134 high path-loss exponent, whereas the Voronoi tessellation nat-
 135 urally emerges from the random BS distribution model, again

provided that the path-loss exponent is sufficiently high. How- 136
 ever, such a high path-loss exponent is unrealistic in real trans- 137
 mission environments. Therefore, our physical analysis reveals 138
 the fundamental limitation of these purely graphic-based cellu- 139
 lar topologies, namely, lack of the connection to the underlying 140
 signal transmission medium. In fact, we demonstrate that the 141
 cell edge boundary shows irregular near-circular shapes, given a 142
 more realistic path-loss exponent of around 3, which cannot be 143
 modeled accurately by either hexagonal or Voronoi tessellation. 144

2) *EUDPE-Based Other-Cell Interference Model:* We pro- 145
 pose a universal model for evaluating the other-cell interfer- 146
 ence, which we refer to as the equivalent uniform-density 147
 plane-entity (EUDPE) method. This generic EUDPE model can 148
 be used to calculate the cumulative other-cell interference for 149
 all the existing BS distribution models that can be found in 150
 practice, including both stochastic and deterministic cellular 151
 network models, such as the stochastic Poisson distributed (PD) 152
 and uniformly distributed (UD) BS models and the determinis- 153
 tic grid-based BS model. 154

3) *Lower Bound Analysis for Coverage Probability and* 155
Average Achievable Rate: Based on the proposed generic 156
 EUDPE interference model, we perform the low-bound anal- 157
 ysis of both the coverage probability and the average achiev- 158
 able rate for various BS distribution models, specifically, the 159
 stochastic PD and UD BS models and the deterministic grid- 160
 based BS model, which may be viewed as a degenerated or spe- 161
 cial case of the UD BS model. For realistic path-loss exponents, 162
 the coverage probability and average achievable throughput 163
 results provided by our proposed analysis approach agree with 164
 the simulated coverage probability and achievable throughput. 165
 In fact, their match is as good or better than that of the PPP- 166
 based analysis. The results also show that the noise only has a 167
 modest effect on the coverage probability and achievable rate. 168

The remainder of this paper is organized as follows. In 169
 Section II, the downlink cellular system model is briefly in- 170
 troduced, which is followed by our new physical analysis of 171
 cell edge boundary. Section III is devoted to the derivation of 172
 our EUDPE-based interference model. The low-bound analysis 173
 of the coverage probability based on the EUDPE method is 174
 deduced in Section IV for both stochastic BS distribution 175
 models and deterministic grid-based BS models, whereas the 176
 corresponding low-bound analysis is presented in Section V. 177
 Our conclusions are offered in Section VI. 178

179 II. DOWNLINK CELLULAR SYSTEM MODEL

Throughout our discussions, the index set of the BSs, which 180
 are deployed according to some distribution, is denoted by Φ , 181
 whereas the serving BS's index is denoted by b_0 . Furthermore, 182
 the average density of BSs is ρ . Let P be the transmitted power 183
 of a BS, R be the serving BS's coverage radius, R_{nw} be the 184
 distance from the serving BS to the edge of the network, and 185
 r_i denotes the distance from the i th BS to the user equipment 186
 (UE) concerned. If we denote the average coverage area of a 187
 BS by $\mathbb{E}[A_s]$ with $\mathbb{E}[\cdot]$ representing the expectation operator, 188
 then $\mathbb{E}[A_s] = 1/\rho$. We will also use $2R$ to denote the average 189
 distance between two neighboring BSs, and we have $R \propto 190$
 $\sqrt{\mathbb{E}[A_s]}$. 191

¹The simulation results are referred to as "experimental" or "actual" in [12], which is inappropriate.

192 A. SINR Model

193 The wireless channel linking the i th BS and the UE con-
 194 sidered is modeled by a complex-valued channel tap that takes
 195 into account the path loss with a path-loss exponent of α , the
 196 fast Rayleigh fading coefficient with an instantaneous power
 197 or a squared magnitude of h_i , and the channel's additive white
 198 Gaussian noise (AWGN) with noise power of σ^2 . The average
 199 of the random variable h_i is denoted by \bar{h} ; therefore, h_i follows
 200 the exponential distribution with the mean \bar{h} .

201 Let us assume that the intracell UE-to-UE interference is neg-
 202 ligible. Then, the signal-to-interference-plus-noise ratio (SINR)
 203 experienced at this UE can be expressed as follows:

$$\text{SINR} = \frac{Ph_0r_0^{-\alpha}}{I_r + \sigma^2} \quad (1)$$

204 where the interference arriving from all the interfering cells is
 205 given by

$$I_r = \sum_{i \in \Phi \setminus b_0} Ph_i r_i^{-\alpha}. \quad (2)$$

206 If the target SINR value is T , then the actual SINR must obey
 207 $\text{SINR} > T$, which requires

$$h_0 > P^{-1}Tr_0^\alpha (\sigma^2 + I_r). \quad (3)$$

208 Thus, the probability distribution of h_0 should be taken into
 209 account in the analysis of both the coverage probability and the
 210 average rate. Furthermore, intuitively, the given SINR model
 211 determines the coverage area of each BS; therefore, it influences
 212 the cell shape or boundary.

213 B. Physical Analysis of Cell Edge Boundary

214 As aforementioned, the grid-based cellular model is conve-
 215 nient but is too idealistic. By contrast, the Voronoi tessellation is
 216 considered to match the random BS deployment in relative flat
 217 urban areas reasonably well [12], [23]. Hence, cellular networks
 218 can be analyzed using Voronoi diagram theory, albeit this has
 219 not been explained with the aid of a physically tangible per-
 220 spective. More specifically, both the energy efficiency and cov-
 221 erage of cellular networks may be analyzed based on Voronoi
 222 tessellation [24], [25]. Fig. 1 shows a random distribution of
 223 the BSs with the cell boundaries corresponding to a Voronoi
 224 tessellation. Note that in both the grid-based and Voronoi-based
 225 cellular topologies, the cell boundaries are determined purely
 226 by the geometric property of the BS distribution, and they are
 227 completely independent of the actual physical interference that
 228 the network is experiencing.

229 To interpret the cell edge boundary from a physical percep-
 230 tively, namely, linking it better to the underlying physics of
 231 signal transmission medium, let us now introduce the following
 232 definition that formally defines the cell edge boundary.

233 *Definition 1:* The cell edge boundary is constituted by the
 234 group of points where the strength of the desired signal received
 235 from the serving BS equals to the interfering signal's strength.
 236 In other words, at the cell edge boundary, the desired signal-
 237 to-interference ratio (SIR) is equal to 1. This definition of cell

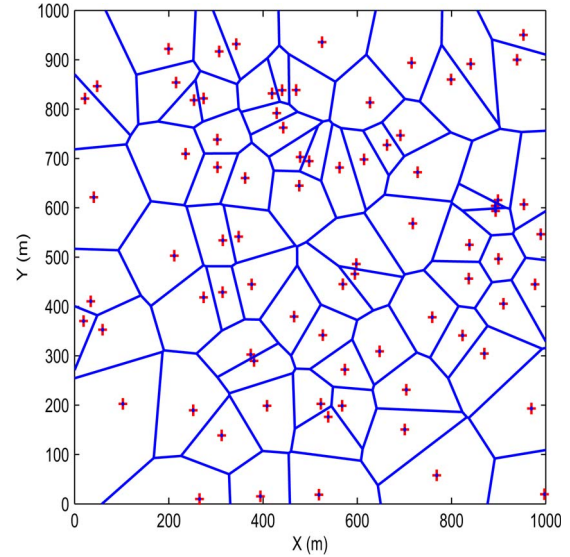


Fig. 1. Random distribution of the BSs marked by +, with the cell boundaries corresponding to a Voronoi tessellation.

edge boundary is both intuitive and practical since, within the
 238 coverage area of a BS, the desired signal should be stronger than
 239 the interfering signal, yielding $\text{SIR} > 1$. Let us denote the i th
 240 BS location as the point z_i , where $i \in \Phi$. Furthermore, denote
 241 the distance from z_i to a point z as $|z - z_i|$. The desired signal
 242 power at the point z provided by the i th BS is given by
 243

$$S(z) = \mathbb{E} [Ph_i |z - z_i|^{-\alpha}] = P\bar{h} |z - z_i|^{-\alpha} \quad (4)$$

while the interfering signal's power at z is given by
 244

$$\begin{aligned} I(z) &= \mathbb{E} [I_r(z)] = \mathbb{E} \left[\sum_{j \in \Phi \setminus i} Ph_j |z - z_j|^{-\alpha} \right] \\ &= P\bar{h} \sum_{j \in \Phi \setminus i} |z - z_j|^{-\alpha}. \end{aligned} \quad (5)$$

Thus, with respect to the i th BS, the SIR at the point z is 245
 given by
 246

$$\text{SIR}(z) = \frac{|z - z_i|^{-\alpha}}{\sum_{j \in \Phi \setminus i} |z - z_j|^{-\alpha}}. \quad (6)$$

Therefore, at the i th cell's edge boundary, we have $\text{SIR}(z) = 1$. 247

In Figs. 2 and 3, the distribution of the BSs is based on the
 248 same regular grid network model, and the number of BSs is 33. 249
 As shown in Fig. 2, the shape of each cell in the network is 250
 approximately a regular circle given the path-loss exponent of 251
 $\alpha = 3$. By contrast, observe in Fig. 3 that the cell shape changes 252
 into a hexagonal one when the path-loss exponent is increased 253
 to $\alpha = 10$. 254

In Figs. 4 and 5, the locations of the 33 BSs are randomly 255
 drawn from the uniform distribution across the entire network 256
 area. The cells now approximately have irregularly circular 257
 shapes when the path-loss exponent is $\alpha = 3$, but interestingly, 258
 it is the Voronoi tessellation that naturally emerges when the 259
 path-loss exponent is increased to $\alpha = 10$. 260

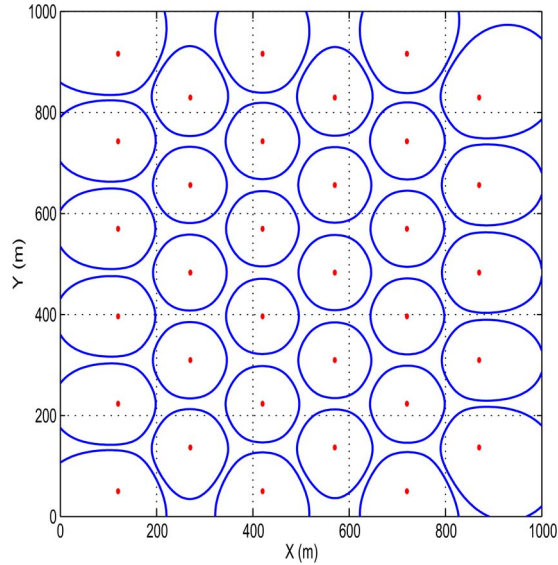


Fig. 2. Cell edge boundaries of the grid network model with the 33 BS locations marked by dots, as determined by $SIR(z) = 1$. The path-loss exponent is $\alpha = 3$.

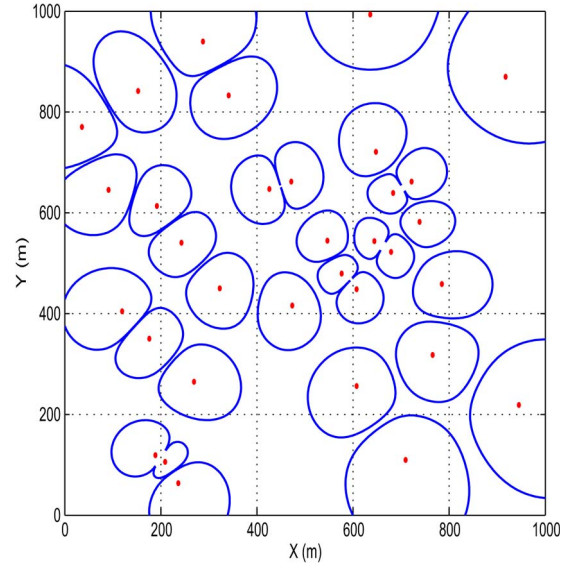


Fig. 4. Cell edge boundaries of the randomly distributed network model with the 33 BS locations marked by dots, as determined by $SIR(z) = 1$. The path-loss exponent is $\alpha = 3$.

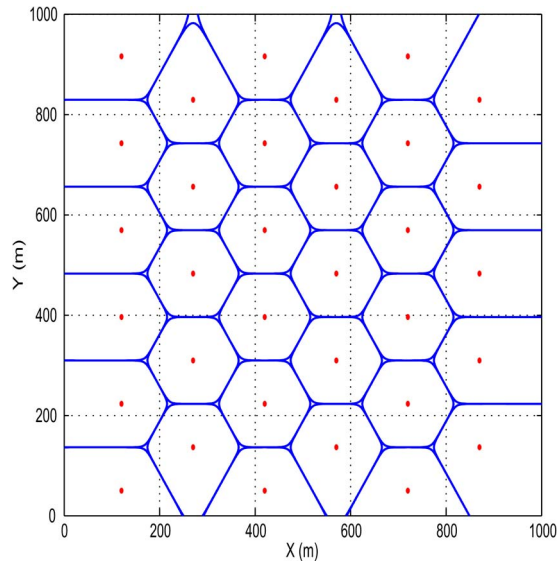


Fig. 3. Cell edge boundaries of the grid network model with the 33 BS locations marked by dots, as determined by $SIR(z) = 1$. The path-loss exponent is $\alpha = 10$.

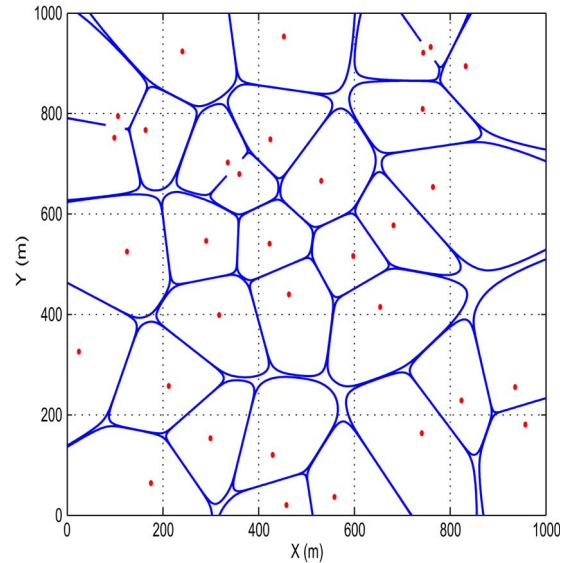


Fig. 5. Cell edge boundaries of the randomly distributed network model with the 33 BS locations marked by dots, as determined by $SIR(z) = 1$. The path-loss exponent is $\alpha = 10$.

261 The given results demonstrate that our Definition 1 of cell
 262 edge boundary is a physically plausible one for analyzing the
 263 network, and both the hexagonal topology and the Voronoi
 264 tessellation naturally emerge according to this definition, de-
 265 pending on whether the geographic distribution of BSs is deter-
 266 ministic or random and providing that the path-loss exponent
 267 is sufficiently high. Note that such a high path-loss exponent
 268 is unrealistic in real transmission environments. Therefore,
 269 our analysis of cell edge boundary reveals a weakness of the
 270 popular hexagonal and Voronoi network topologies, namely,
 271 they do not reflect the underlying signal transmission medium.
 272 Significantly, given a more realistic path-loss exponent of ap-
 273 proximately three, the cell edge boundary exhibits irregular

near-circular cell shapes, for which neither hexagonal topology 274
 nor Voronoi tessellation can be used to accurately model. 275
 Furthermore, the “weak” coverage areas that are left outside 276
 any cell boundary, where the desired signal is weaker than the 277
 interfering signals, as shown in Fig. 4, highlight the benefits of 278
 employing collaborative relaying techniques. 279

III. EQUIVALENT UNIFORM DENSITY PLANE-ENTITY FOR 280 CUMULATIVE INTERFERENCE CALCULATION 281

To accurately analyze the coverage probability and the 282
 achievable rate, it is necessary to find an efficient means for 283

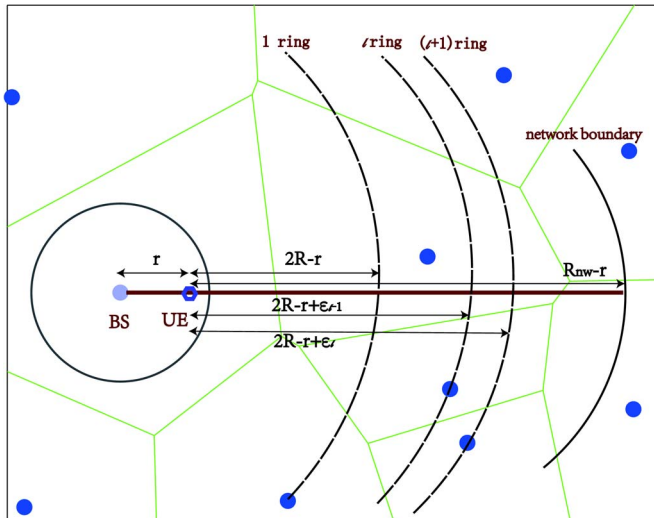


Fig. 6. Proposed EUDPE method for calculating the other-cell interference.

284 cumulative interference calculation. By considering the dis-
 285 tribution of the interference imposed by the BSs in the law
 286 of large numbers and combining it with the fluid model of
 287 [26], we propose the EUDPE method for calculating the cu-
 288 mulative interference. The basic idea of this EDUPE method
 289 is as follows. Although the actual geographic distribution of
 290 BSs always shows a certain degree of irregularity, we may
 291 define a group of equivalent and uniformly distributed BSs for
 292 approximating the other-cell CCI. Since, in real-world cellular
 293 networks, the actual geographic distribution of BSs is often
 294 close to a uniform random distribution, such an approximation
 295 is sufficiently accurate. It is worth emphasizing however that
 296 we do not assume a uniform and random BS distribution for
 297 the actual network to be modeled. More specifically, given
 298 a network having the average BS density of ρ , we approx-
 299 imate this network with an equivalent network whose BSs
 300 are uniformly distributed and whose BS density is also ρ .
 301 Such a network is termed the equivalent EUDPE of the given
 302 network. With the aid of our EUDPE method, we can calcu-
 303 late or approximate the cumulative interference for any given
 304 network.

305 Fig. 6 illustrates the concept of the EUDPE, where the
 306 serving BS is assumed the origin of the polar coordinate plane.
 307 Since the coverage radius of a BS is R , the distance between
 308 two neighboring BSs is $2R$, where $R \propto (1/\sqrt{\rho})$. For notational
 309 simplification, we drop the subscript 0 from r_0 and denote the
 310 distance from the serving BS to the UE as r , where $0 \leq r \leq R$.
 311 Thus, the distance from the nearest interfering BS to the UE
 312 is $(2R - r)$. As shown in Fig. 6, the network's coverage area
 313 is partitioned by the N_r rings, and the distance from the UE
 314 to the l th ring is given by $(2R - r + \varepsilon_{l-1})$, where $1 \leq l \leq$
 315 N_r with $\varepsilon_0 = 0$ and $(2R - r + \varepsilon_{N_r}) = R_{nw} - r$. The number
 316 of BSs within the area between the l th and $(l + 1)$ th rings
 317 is approximately $\int_0^{2\pi} \int_{2R-r+\varepsilon_{l-1}}^{2R-r+\varepsilon_l} \rho z dz d\theta$ when assuming the
 318 equivalent EUDPE having the BS density of ρ . Furthermore,
 319 each of these equivalent BSs has the same instantaneous
 320 fast fading channel power of \tilde{h}_l , and the mean of \tilde{h}_l is \bar{h} .

Thus, the cumulative interference I_r can be approximated 321
 according to 322

$$I_r = \sum_{l=1}^{N_r} \int_0^{2\pi} \int_{2R-r+\varepsilon_{l-1}}^{2R-r+\varepsilon_l} P\tilde{h}_l z^{-\alpha} \rho z dz d\theta$$

$$= \sum_{l=1}^{N_r} \frac{2\pi\rho P\bar{h}_l}{\alpha-2} \left((2R-r+\varepsilon_{l-1})^{2-\alpha} - (2R-r+\varepsilon_l)^{2-\alpha} \right). \quad (7)$$

Theorem 1: The average of I_r is given by 323

$$\mathbb{E}[I_r] = \frac{2\pi\rho P\bar{h}}{\alpha-2} \left((2R-r)^{2-\alpha} - (R_{nw}-r)^{2-\alpha} \right). \quad (8)$$

Proof: According to the Campbell-Mecke theorem [27], 324
 we have 325

$$\mathbb{E} \left[\sum_{l=1}^{N_r} \frac{2\pi\rho P\tilde{h}_l}{\alpha-2} \left((2R-r+\varepsilon_{l-1})^{2-\alpha} - (2R-r+\varepsilon_l)^{2-\alpha} \right) \right]$$

$$= \sum_{l=1}^{N_r} \frac{2\pi\rho P\mathbb{E}[\tilde{h}_l]}{\alpha-2} \left((2R-r+\varepsilon_{l-1})^{2-\alpha} - (2R-r+\varepsilon_l)^{2-\alpha} \right)$$

$$= \frac{2\pi\rho P\bar{h}}{\alpha-2} \left((2R-r)^{2-\alpha} - (R_{nw}-r)^{2-\alpha} \right). \quad (9)$$

■ 326

Typically, the path-loss exponent is $\alpha > 2$ in realistic net- 327
 works. Noting that $(R_{nw}-r)^{2-\alpha} \rightarrow 0$ as $R_{nw} \rightarrow +\infty$, we 328
 have the following corollary. 329

Corollary 1: Given that the network's boundary is suffi- 330
 ciently far away, namely, $R_{nw} \rightarrow +\infty$, we have 331

$$\mathbb{E}[I_r] = \frac{2\pi\rho P\bar{h}}{\alpha-2} (2R-r)^{2-\alpha}. \quad (10)$$

IV. COVERAGE PROBABILITY ANALYSIS USING 332 EQUIVALENT UNIFORM DENSITY PLANE-ENTITY 333

As mentioned earlier, the cellular system interference model 334
 and the BS geographic distribution model are required in cov- 335
 erage analysis. Our proposed EUDPE is a universal method 336
 for evaluating the other-cell interference for all existing BS 337
 distribution models, such as the stochastic PD and UD BS 338
 models and the deterministic grid-based model. 339

A. Coverage Probability Analysis Using EUDPE-PD 340

Since a popular geographic BS distribution is the Poisson 341
 distribution [12]–[15], we first consider the PD BS model. The 342
 probability density function (pdf) of the Poisson distribution 343
 can be derived using the method of [28]. Let λ be the intensity 344
 of the Poisson distribution that models the BS geographic 345
 distribution and R be the average coverage radius of a cell. 346
 Then, the probability of having no BS that is closer than x is 347
 given by 348

$$\mathbb{P}\{r > x\} = \mathbb{P}\{\text{No BS closer than } x\} = e^{-\lambda\pi x^2}. \quad (11)$$

349 The corresponding cumulative distribution function (cdf) is
350 then given by

$$\mathbb{P}\{r \leq x\} = F(x) = 1 - e^{-\lambda \pi x^2}. \quad (12)$$

351 Therefore, the pdf is defined as

$$f(r) = \frac{dF(r)}{dr} = 2\pi\lambda r e^{-\pi\lambda r^2}. \quad (13)$$

352 Given the SINR threshold T , the intensity λ and the path-loss
353 exponent α , the coverage probability is defined as

$$\begin{aligned} p_c(T, \lambda, \alpha) &= \mathbb{E}_r [\mathbb{E}_{I_r} [\mathbb{P}\{\text{SINR} > T\}]] \\ &= \int_{r>0} \mathbb{E}_{I_r} [\mathbb{P}\{h_0 > P^{-1}Tr^\alpha(\sigma^2 + I_r)\}] 2\pi\lambda r e^{-\pi\lambda r^2} dr \end{aligned} \quad (14)$$

354 where $\mathbb{E}_r[\bullet]$ denotes the expectation with respect to the random
355 variable r .

356 1) *Lower Bound for the Probability of SINR Larger Than*
357 *Threshold:* Noting that h_0 obeys the exponential distribution
358 with the mean \bar{h} , the probability of the SINR larger than the
359 threshold T (averaged over the interference) is given by

$$\begin{aligned} \mathbb{E}_{I_r} [\mathbb{P}\{h_0 > P^{-1}Tr^\alpha(\sigma^2 + I_r)\}] \\ = e^{-\bar{h}P^{-1}Tr^\alpha\sigma^2} \mathbb{E}_{I_r} [e^{-\bar{h}P^{-1}Tr^\alpha I_r}]. \end{aligned} \quad (15)$$

360 *Theorem 2:* A lower bound for the probability of the SINR
361 greater than the threshold T is expressed as

$$\mathbb{E}_{I_r} [\mathbb{P}\{h_0 > P^{-1}Tr^\alpha(\sigma^2 + I_r)\}] \geq e^{-\bar{h}Tr^\alpha\eta(\alpha, r)} \quad (16)$$

362 where

$$\eta(\alpha, r) = P^{-1}\sigma^2 + \frac{2\pi\rho\bar{h}}{\alpha-2} ((2R-r)^{2-\alpha} - (R_{\text{nw}}-r)^{2-\alpha}). \quad (17)$$

363 *Proof:* According to Jensen's inequality [29], we have

$$\mathbb{E}_{I_r} [e^{-\bar{h}P^{-1}Tr^\alpha I_r}] \geq e^{-\bar{h}P^{-1}Tr^\alpha \mathbb{E}[I_r]}. \quad (18)$$

364 Substituting (18) into (15) and noting $\mathbb{E}[I_r]$ of (8) leads to (16)
365 with $\eta(\alpha, r)$ given in (17). ■

366 *Corollary 2:* Given that the network boundary is sufficiently
367 far away, namely, $R_{\text{nw}} \rightarrow +\infty$

$$\mathbb{E}_{I_r} [\mathbb{P}\{h_0 > P^{-1}Tr^\alpha(\sigma^2 + I_r)\}] \geq e^{-\bar{h}Tr^\alpha\xi(\alpha, r)} \quad (19)$$

368 where

$$\xi(\alpha, r) = P^{-1}\sigma^2 + \frac{2\pi\rho\bar{h}}{\alpha-2} (2R-r)^{2-\alpha}. \quad (20)$$

369 2) *Lower Bound for the Coverage Probability:* A lower
370 bound for the coverage probability $p_c(T, \lambda, \alpha)$ is given by the
371 following theorem.

Theorem 3: For the network where the BS geographic
distribution obeys the Poisson distribution of intensity λ ,
a lower bound for the coverage probability $p_c(T, \lambda, \alpha)$ is
given by

$$p_{cl}(T, \lambda, \alpha) = \pi\lambda \int_0^{R^2} e^{-\bar{h}Tv^{\alpha/2}\psi(\alpha, v) - \pi\lambda v} dv \quad (21)$$

where R is the coverage radius of the serving BS, and

$$\begin{aligned} \psi(\alpha, v) &= P^{-1}\sigma^2 + \frac{2\pi\rho\bar{h}}{\alpha-2} \left((2R - v^{1/2})^{2-\alpha} \right. \\ &\quad \left. - (R_{\text{nw}} - v^{1/2})^{2-\alpha} \right). \end{aligned} \quad (22)$$

Proof: From (14) and Theorem 2, as well as noting that
 $r \leq R$, we have

$$p_{cl}(T, \lambda, \alpha) = \int_0^R 2\pi\lambda r e^{-\bar{h}Tr^\alpha\eta(\alpha, r) - \pi\lambda r^2} dr. \quad (23)$$

By defining $r^2 = v$, (23) is transformed into (21) with $\psi(\alpha, v)$
given in (22). ■

Corollary 3: Given that the network boundary is sufficiently
far away, namely, $R_{\text{nw}} \rightarrow +\infty$, a lower bound for the coverage
probability $p_c(T, \lambda, \alpha)$ is expressed as

$$p_{cl}(T, \lambda, \alpha) = \pi\lambda \int_0^{R^2} e^{-\bar{h}Tv^{\alpha/2}\chi(\alpha, v) - \pi\lambda v} dv \quad (24)$$

where

$$\chi(\alpha, v) = P^{-1}\sigma^2 + \frac{2\pi\rho\bar{h}}{\alpha-2} (2R - v^{1/2})^{2-\alpha}. \quad (25)$$

Remark 1: In the coverage analysis for the EUDPE-PD
model, the average coverage radius R is related to the average
cell area $\mathbb{E}[A_s]$. Noting $R \propto \sqrt{\mathbb{E}[A_s]}$ and $\mathbb{E}[A_s] = 1/\rho$, we
may use

$$R = \frac{c_f}{\sqrt{\rho}} \quad (26)$$

where c_f is an empirically chosen factor. For example, if the
average cell is defined by a square shape, we have $\mathbb{E}[A_s] = 4R^2$;
therefore, we have $c_f = 1/2 = 0.5$. On the other hand, if the
average coverage area is calculated according to a hexagonal
one, we have $\mathbb{E}[A_s] = 2\sqrt{3}R^2$, yielding $c_f = 1/\sqrt{2\sqrt{3}} \approx 0.54$,
whereas for the average circle-shape cell, we have $c_f = 1/\sqrt{\pi} \approx 0.56$.

B. Coverage Probability Analysis Using EUDPE-UD

For many practical cellular networks, the geographic BS
distribution is often close to a uniform random distribution.
Therefore, we next consider the UD BS model with the average

400 density of BSs given by ρ . In this case, the corresponding cdf is
401 given by

$$\mathbb{P}\{z \leq x\} = F(x) = \frac{x^2}{c_{\text{nm}}^2} \rho, \quad 0 \leq x \leq R \quad (27)$$

402 where c_{nm}^2 is a normalization factor, and R is the coverage
403 radius of the serving BS. Thus, the pdf is given as

$$f(r) = \frac{2\rho}{c_{\text{nm}}^2} r, \quad 0 \leq r \leq R. \quad (28)$$

404 The normalization factor c_{nm}^2 is determined as follows. Assume
405 that $E[A_s] = R^2/c_f^2$, where c_f is defined in (26), and fur-
406 ther note that $E[A_s] = 1/\rho$. From $\int_0^R f(r) dr = 1$, we obtain
407 $c_{\text{nm}}^2 = c_f^2$.

408 The coverage probability is therefore defined as

$$\begin{aligned} p_c(T, \rho, \alpha) &= \mathbb{E}_r [\mathbb{E}_{I_r} [\mathbb{P}\{\text{SINR} > T\}]] \\ &= \frac{\rho}{c_f^2} \int_0^R \mathbb{E}_{I_r} [\mathbb{P}\{h_0 > P^{-1} T r^\alpha (\sigma^2 + I_r)\}] 2r dr. \end{aligned} \quad (29)$$

409 A lower bound of $\mathbb{E}_{I_r} [\mathbb{P}\{h_0 > P^{-1} T r^\alpha (\sigma^2 + I_r)\}]$ is given in
410 Theorem 2. Similar to the case of the EUDPE-PD expressed in
411 Theorem 3, therefore, a lower bound for the coverage probabil-
412 ity $p_c(T, \rho, \alpha)$ is given by the following theorem.

413 *Theorem 4:* For the network where the BS geographic distri-
414 bution obeys the uniform random distribution with an average
415 BS density of ρ , a lower bound for the coverage probability
416 $p_c(T, \rho, \alpha)$ is given by

$$p_{cl}(T, \rho, \alpha) = \frac{\rho}{c_f^2} \int_0^{R^2} e^{-\bar{h} T v^{\alpha/2} \psi(\alpha, v)} dv \quad (30)$$

417 where $\psi(\alpha, v)$ is defined in (22).

418 *Corollary 4:* Given that the network boundary is sufficiently
419 far away, a lower bound for the coverage probability $p_c(T, \rho, \alpha)$
420 is expressed by

$$p_{cl}(T, \rho, \alpha) = \frac{\rho}{c_f^2} \int_0^{R^2} e^{-\bar{h} T v^{\alpha/2} \chi(\alpha, v)} dv \quad (31)$$

421 where $\chi(\alpha, v)$ is defined in (25).

422 *Remark 2:* How to set the average coverage radius R is
423 explained in Remark 1. Specifically, we may use $R = c_f/\sqrt{\rho}$,
424 where c_f is an empirically chosen factor.

425 C. Coverage Probability Analysis Using EUDPE-Grid

426 With the aid of the EUDPE method, it is straightforward to
427 carry out the coverage probability analysis for all the traditional
428 deterministic grid-based cellular network models, such as the
429 squared and hexagonal ones. This is because the coverage
430 probability analysis using the EUDPE-Grid model is simply a
431 degenerated or special case of the EUDPE-UD-based analysis,

where the density of BSs ρ is identical everywhere in the net- 432
work, and every cell has the identical shape with the same area 433
 A_s . Therefore, the lower bounds of the coverage probability for 434
the finite-size and infinite-size grid-based network models are 435
given in Theorem 4 and Corollary 4, respectively. Moreover, 436
choosing $R = 1/(2\sqrt{\rho})$ corresponds to the grid-based network 437
with squared cells, whereas using $R = 1/(\sqrt{2\sqrt{3}}\sqrt{\rho})$ is related 438
to considering the grid-based network with hexagonal cells. In 439
general, we may use $R = c_f/\sqrt{\rho}$ for any deterministic grid- 440
based network by choosing an appropriate value for c_f . It be- 441
comes obvious that, under the equivalent network environment 442
of the same ρ and R values, the coverage probability obtained 443
by the EUDPE-Grid-based analysis is identical to that obtained 444
by the EUDPE-UD-based analysis. 445

D. Numerical Results for Coverage Probability

446

We evaluated the coverage probability first by simulation and 447
used the simulated results as the benchmark for the comparison 448
with our theoretical analytic results. We considered two sce- 449
narios. The first case is a single-tier network constructed by 450
macrocells, obeying the uniform random BS distribution and 451
the cellular channel model described in Section II, whereas 452
the second network followed a Poisson BS distribution and 453
obeyed the same cellular channel model of Section II. Given 454
the SINR threshold T , the path-loss exponent α , and the SINR 455
value, the simulated coverage probability was calculated using 456
the pseudocodes presented in Algorithm 1. In the simulation, 457
we set the number of BSs to $N_{\text{BS}} = 80$, the number of UEs to 458
 $N_{\text{UE}} = 10\,000$, the network coverage area to Network Area = 459
 $1000 \times 1000 \text{ m}^2$, and the number of sample simulations to 460
 $N_{\text{max}} = 100$. The average density of BSs was then given as 461

$$\rho = \frac{N_{\text{BS}}}{\text{Network Area}} [\text{BSs/m}^2]. \quad (32)$$

For the Poisson distribution, its intensity was $\lambda = \rho$. We com- 462
pared our low-bound coverage probability results based on the 463
EUDPE-PD and EUDPE-UD models with that of the PPP- 464
based analysis [12]. Since the PPP method can only consider 465
the case of an infinitely large network, we assumed the network 466
boundary $R_{\text{nw}} \rightarrow +\infty$. In the following comparison, the simu- 467
lation results obtained by the network with the uniform random 468
BS distribution are labeled as Simulated data 1, whereas the 469
simulation results yielded by the network with the Poisson BS 470
distribution are denoted Simulated data 2. 471

Algorithm 1 Network Simulation to Evaluate the Coverage Probability.

- 1: Give the number of BSs N_{BS} , the Network Area, and the 472
number of UEs N_{UE} ; 473
- 2: Give the maximum number of sample simulations N_{max} ; 474
- 3: Set Average Coverage Probability = 0; 475
- 4: **for** $N_{\text{sm}} = 1$ to N_{max} **do** 476
- 5: Uniformly and randomly draw the N_{BS} BSs over Net- 477
work Area, or draw the N_{BS} BSs over Network Area by 478
the Poisson distribution; 479

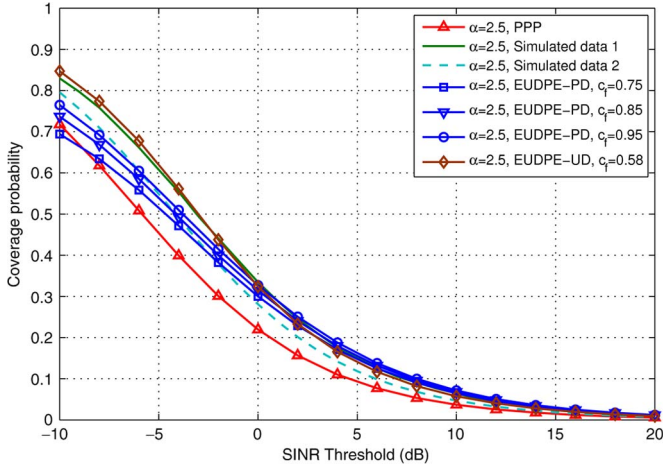


Fig. 7. Comparison of the coverage probabilities based on three different models to the network simulation results, given the path-loss exponent of $\alpha = 2.5$ and no noise, i.e., the AWGN power $\sigma^2 = 0$ and $\text{SINR} = \text{SIR}$.

```

480 6: Uniformly and randomly draw the  $N_{\text{UE}}$  UEs over Net-
481     work Area;
482 7: Initialization: count = 0;
483 8: for  $j = 1$  to  $N_{\text{UE}}$ , do
484 9:     if  $\text{SINR}_j \geq T$  then
485 10:        count = count + 1;
486 11:     end if
487 12: end for
488 13: Coverage Probability = count/ $N_{\text{UE}}$ ;
489 14: Average Coverage Probability +=
490     Coverage Probability;
491 15: end for
492 16: Average Coverage Probability / =  $N_{\text{max}}$ .

```

493 Given the path-loss exponent of $\alpha = 2.5$ and assuming no
494 AWGN or $\sigma^2 = 0$, which implies $\text{SINR} = \text{SIR}$, Fig. 7 shows
495 the coverage probabilities calculated based on the three analytic
496 models, in comparison to the coverage probabilities obtained by
497 the two different network simulations, when varying the SINR
498 threshold. It is shown in Fig. 7 that the coverage probability
499 analysis results of our proposed EUDPE-PD and EUDPE-UD
500 models agree with both simulation results well, better than the
501 PPP-based analysis. When the path-loss exponent is increased
502 to $\alpha = 3$ and 4, the results obtained are shown in Figs. 8
503 and 9, respectively, where it can be seen that the EUDPE-
504 UD analysis agrees with the simulation result based on the
505 network with the uniform random BS distribution better than
506 the other two models, whereas the PPP-based analysis agrees
507 better with the simulation result of the network with the Poisson
508 BS distribution better than the other two models.

509 It is worth emphasizing that because there exist no real
510 network performance data to validate an analysis model, we
511 can only rely on the simulated data. When we have an analysis
512 model agrees with a particular simulation result better than an-
513 other analysis model, it does not imply that the former is better
514 than the latter. The particular simulation result may not actually
515 represent the true real network performance and, moreover, the
516 simulation conditions may not actually match those imposed
517 on an analysis model. What we can claim however is that, if

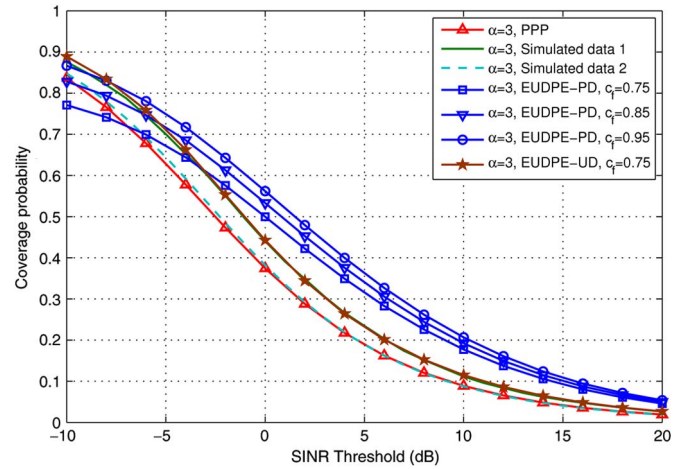


Fig. 8. Comparison of the coverage probabilities based on three different models to the network simulation results, given the path-loss exponent of $\alpha = 3$ and no noise, i.e., the AWGN power $\sigma^2 = 0$ and $\text{SINR} = \text{SIR}$.

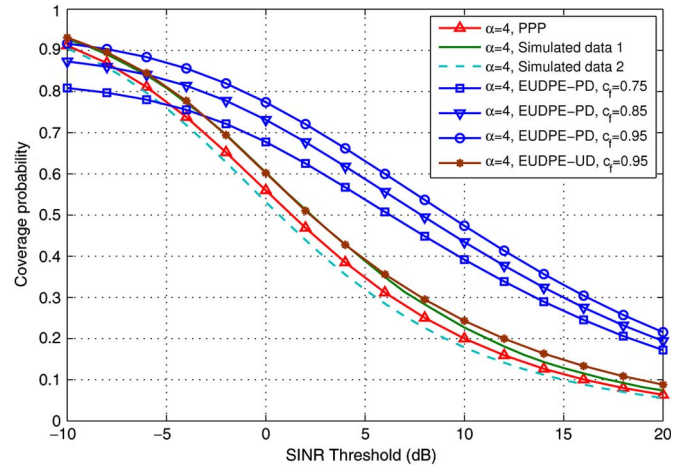


Fig. 9. Comparison of the coverage probabilities based on three different models to the network simulation results, given the path-loss exponent of $\alpha = 4$ and no noise, i.e., the AWGN power $\sigma^2 = 0$ and $\text{SINR} = \text{SIR}$.

an analysis model agrees well with simulation data, it is a rea- 518
519 sonable tool for network analysis and planning. Similarly, if a
520 lower bound coverage probability derived by an analysis model
521 appears to be larger than a simulated coverage probability, it
522 does not imply that this analysis model is wrong. Again, the
523 simulation conditions may not actually match those imposed
524 on the analysis model. For example, we assumed that the
525 network boundary $R_{\text{nw}} \rightarrow +\infty$ for the proposed EUDPE-PD
526 and EUDPE-UD models and the PPP-based analysis for the fair
527 comparison of the three analysis models since the PPP method
528 can only be applied for the case of an infinitely large network.
529 However, the simulated network size was $1000 \times 1000 \text{ m}^2$ and
530 not infinitely large. As shown earlier, another advantage of
531 our analysis approach over the PPP-based method is that our
532 method can be applied to analyze finite-size networks.

In our EUDPE-based analysis, the empirical chosen factor 533
534 c_f is related to the average cell shape and size. The theoretical
535 explanations of this area factor c_f are given in Remark 1.
536 Observe from Fig. 7 that, for the path-loss exponent $\alpha = 2.5$, an
537 appropriate value of this area factor for our EUDPE-UD model
538 is $c_f = 0.58$, which is, in fact, close to the case of the average 538

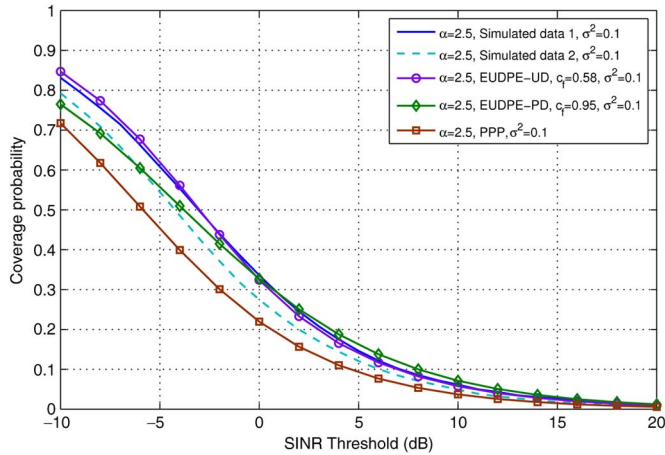


Fig. 10. Comparison of the coverage probabilities based on three different models to the network simulation results, given the path-loss exponent of $\alpha = 2.5$ and the AWGN power $\sigma^2 = 0.1$.

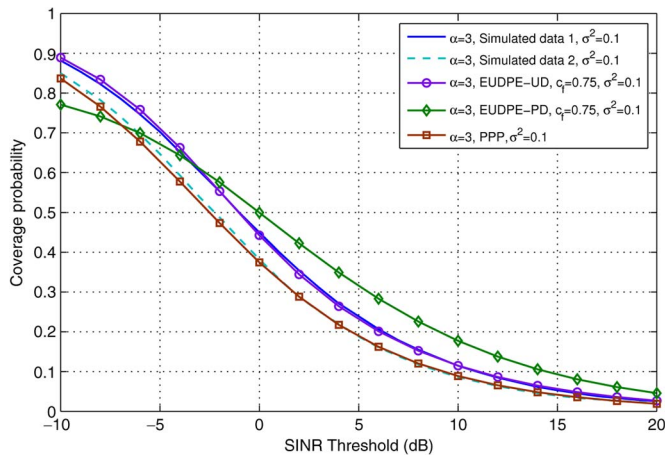


Fig. 11. Comparison of the coverage probabilities based on three different models to the network simulation results, given the path-loss exponent of $\alpha = 3$ and the AWGN power $\sigma^2 = 0.1$.

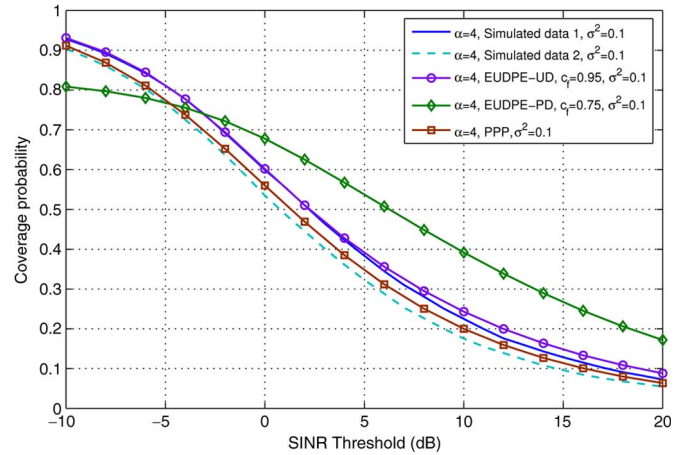


Fig. 12. Comparison of the coverage probabilities based on three different models to the network simulation results, given the path-loss exponent of $\alpha = 4$ and the AWGN power $\sigma^2 = 0.1$.

on the Poisson BS distribution. Upon comparing Figs. 10–12 559 with Figs. 7–9, it can be seen that the effect of the channel 560 AWGN to the achievable coverage probability is minor. For 561 example, observe that the simulated-data-2 curve in Fig. 7 562 almost matches the simulated-data-2 curve in Fig. 10, whereas 563 the PPP-analysis-based curve in Fig. 7 is almost identical to the 564 PPP-analysis-based curve in Fig. 10. Similarly, the other three 565 coverage probability curves in Fig. 10 also closely match the 566 corresponding coverage probability curves in Fig. 7. 567

V. AVERAGE ACHIEVABLE RATE ANALYSIS USING EQUIVALENT UNIFORM DENSITY PLANE-ENTITY

Let us now apply the proposed EUDPE method to analyze 570 the average achievable throughput. According to Shannon’s 571 theory, under the idealized simplifying condition of having a 572 Gaussian interference owing to the central limit theorem, the 573 average achievable rate is defined as [12] 574

$$C \triangleq \mathbb{E}[\ln(1 + \text{SINR})]. \tag{33}$$

Since we are concerned with the system’s achievable through- 575 put, we will consider the case of the network boundary being 576 sufficiently far away, i.e., $R_{\text{nw}} \rightarrow +\infty$. 577

A. Average Achievable Rate Analysis Using EUDPE-PD

Again, we first consider the case that the geographic BS 579 distribution follows a Poisson distribution, and we have the 580 following result. 581

Theorem 5: For the network where the BS geographic 582 distribution obeys the Poisson distribution of intensity λ , a 583 lower bound for the average achievable throughput is given by 584

$$C_l(\lambda, \alpha) = \pi \lambda \int_0^{R^2} e^{-\pi \lambda v} \left(\int_{t>0} e^{-\bar{h} v^{\alpha/2} (e^t - 1) \chi(\alpha, v)} dt \right) dv \tag{34}$$

where $\chi(\alpha, v)$ is given in (25). 585

539 circle-shaped cell. However, as shown in Figs. 8 and 9, as α 540 increases, the appropriate area factor c_f value also increases. A 541 plausible explanation for this phenomenon is offered as follows. 542 As the path-loss exponent α increases, the effective coverage 543 area R^2/c_f^2 of the serving BS is reduced, and this corresponds 544 to an increase in the area factor c_f .

545 Next, the effect of noise imposed on the achievable coverage 546 probability was investigated by setting the AWGN power to 547 $\sigma^2 = 0.1$ or $10 \log_{10}(1/\sigma^2) = 10$ dB, and the results obtained 548 are given in Figs. 10–12, respectively, for the three differ- 549 ent values of α . For graphic clarity, we only draw a single 550 EUDPE-PD-based coverage probability associated with an ap- 551 propriate area factor c_f value in each of these three figures. 552 Again, the same observations as those drawn for Figs. 7–9 can 553 be made, namely, for the case of $\alpha = 2.5$, the EUDPE-UD- 554 based analysis agrees with the both simulation results better 555 than the PPP-based analysis, whereas for higher α values, the 556 EUDPE-UD analysis matches better with the simulated results 557 based on the uniform random BS distribution, and the PPP- 558 based analysis agrees better with the simulated results based

586 *Proof:* According to [12], we have

$$C(\lambda, \alpha) = \int_0^R 2\pi\lambda r e^{-\pi\lambda r^2} \times \int_{t>0} \mathbb{E}_{I_r} [\mathbb{P}\{h_0 > P^{-1}r^\alpha(e^t - 1)(\sigma^2 + I_r)\}] dt dr. \quad (35)$$

587 Similar to Corollary 2, we have

$$\mathbb{E}_{I_r} [\mathbb{P}\{h_0 > P^{-1}r^\alpha(e^t - 1)(\sigma^2 + I_r)\}] \geq e^{-\bar{h}r^\alpha(e^t-1)\xi(\alpha,r)} \quad (36)$$

588 where $\xi(\alpha, r)$ is defined in (20). Thus, a lower bound of $C(\lambda, \alpha)$
589 is given by

$$C_l(\lambda, \alpha) = \int_0^R 2\pi\lambda r e^{-\pi\lambda r^2} \left(\int_{t>0} e^{-\bar{h}r^\alpha(e^t-1)\xi(\alpha,r)} dt \right) dr. \quad (37)$$

590 By defining $v = r^2$ in (37), we obtain (34). ■

591 *Corollary 5:* In the noise-free case, namely, $\sigma^2 = 0$, a lower
592 bound for the average achievable throughput is

$$C_l(\lambda, \alpha) = \pi\lambda \int_0^{R^2} e^{-\pi\lambda v} \left(\int_{t>0} e^{-\bar{h}v^{\alpha/2}(e^t-1)\bar{\chi}(\alpha,v)} dt \right) dv \quad (38)$$

593 where

$$\bar{\chi}(\alpha, v) = \frac{2\pi\rho\bar{h}}{\alpha-2} (2R - v^{1/2})^{2-\alpha}. \quad (39)$$

594 B. Average Achievable Rate Analysis Using EUDPE-UD

595 Next, we consider the case that the geographic BS distribu-
596 tion follows a uniform random distribution, and we have the
597 following result.

598 *Theorem 6:* For the network where the BS geographic dis-
599 tribution obeys the uniform random distribution with an average
600 BS density of ρ , a lower bound for the average achievable
601 throughput is given by

$$C_l(\rho, \alpha) = \frac{\rho}{c_f^2} \int_0^{R^2} \left(\int_{t>0} e^{-\bar{h}v^{\alpha/2}(e^t-1)\chi(\alpha,v)} dt \right) dv \quad (40)$$

602 where $\chi(\alpha, v)$ is given in (25).

603 *Proof:* Noting that the average achievable throughput is
604 defined as

$$C(\lambda, \alpha) = \frac{\rho}{c_f^2} \int_0^R 2r \times \int_{t>0} \mathbb{E}_{I_r} [\mathbb{P}\{h_0 > P^{-1}r^\alpha(e^t - 1)(\sigma^2 + I_r)\}] dt dr \quad (41)$$

605 the proofs are similar to the proofs for Theorem 5. ■

Corollary 6: In the noise-free case, namely, $\sigma^2 = 0$, a lower
606 bound for the average achievable throughput is 607

$$C_l(\rho, \alpha) = \frac{\rho}{c_f^2} \int_0^{R^2} \left(\int_{t>0} e^{-\bar{h}v^{\alpha/2}(e^t-1)\bar{\chi}(\alpha,v)} dt \right) dv. \quad (42)$$

where $\bar{\chi}(\alpha, v)$ is given in (39). 608

Remark 3: It is straightforward to carry out the average
609 achievable throughput analysis for any deterministic grid-based
610 cellular network model, because the EUDPE-Grid model is a
611 special case of the EUDPE-UD model. Therefore, the lower
612 bound of the average achievable throughput for the grid-based
613 network model is also given in Theorem 6. Moreover, under the
614 equivalent network environment of the same ρ and R values,
615 the lower bound of the average achievable throughput obtained
616 by the EUDPE-Grid-based analysis is identical to that obtained
617 by the EUDPE-UD-based analysis. 618

619 C. Numerical Results for Average Achievable Rate

Assuming a unity frequency reuse factor, we compare the
620 lower bounds of the average achievable throughput obtained
621 by the proposed EUDPE-PD- and EUDPE-UD-based analyses
622 to that of the PPP-based analysis [12] in Fig. 13 by varying
623 the path-loss exponent value. The simulated average achiev-
624 able throughputs obtained from the two network simulations
625 with the uniform random BS distribution and the Poisson BS
626 distribution are labeled as Simulated rate 1 and Simulated
627 rate 2, respectively, and they are also given in Fig. 13 as the
628 benchmark. For our proposed EUDPE-PD and EUDPE-UD-
629 based analysis and the network simulations, both the noise-
630 free and noisy results are presented. However, for the
631 PPP-based average achievable throughput analysis, only the
632 noise-free case is provided in [12]; therefore, in Fig. 13, we only
633 present the noise-free PPP-based result. It can be observed that
634 all the three theoretical analysis based results and the simulation
635 data all reveal that the average achievable throughput increases
636 linearly, as the path-loss exponent increases. More specifically,
637 all the analytical and simulated data have accurate linear fitting.
638 It is also shown in Fig. 13 that our proposed EUDPE-PD-
639 and EUDPE-UD-based analyses agree with the two simulated
640 results better than the PPP-based analysis, particularly for the
641 path-loss exponent $\alpha \leq 4.5$. The results of Fig. 13 also show
642 that the noise only has a minor effect on the average achievable
643 throughput, which is expected as we consider the interference-
644 limited scenario with a unity frequency reuse factor. 645

646 VI. CONCLUSION

We have proposed a universal approach for accurately
647 analyzing the coverage probability and average achievable
648 throughput of cellular networks. More specifically, we have
649 derived a generic EUDPE procedure for evaluating the other-
650 cell interference. Based on this EUDPE interference model, we
651 have derived the lower bounds of both the coverage probability
652 and average achievable throughput for various practical BS
653 distribution models, including the stochastic Poisson distributed
654 model, uniformly and randomly distributed model, and the 655

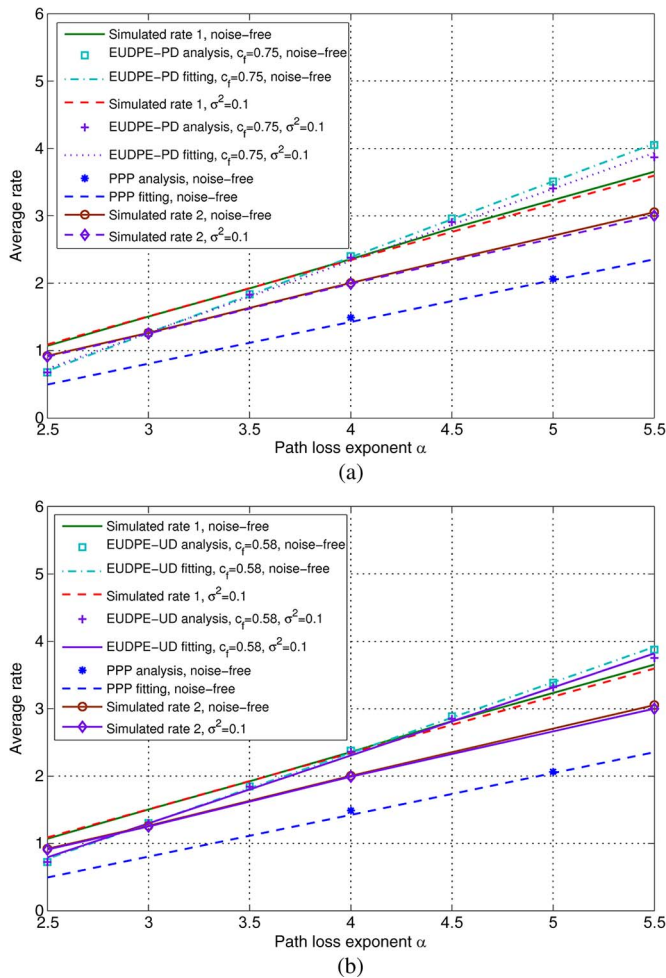


Fig. 13. Comparison of the average achievable throughputs based on three different models to the network simulation results, given different path-loss exponent values. (a) EUDPE-PD and PPP models and (b) EUDPE-UD and PPP models.

656 deterministic grid-based model. Extensive simulation results
 657 have validated that the coverage probability and average
 658 throughput obtained by our proposed universal analysis method
 659 agree with the simulated coverage probability and average
 660 throughput at least as closely as those obtained by the popular
 661 existing PPP-based analysis, if not better. In addition, we have
 662 also introduced a generic and physical definition of cell edge
 663 boundary. We have shown that the popular hexagonal and
 664 Voronoi network topologies only emerge from the grid-based
 665 network model and the random BS distribution model, respec-
 666 tively, given an unrealistic high path-loss exponent according
 667 to this definition. Moreover, we have demonstrated that the cell
 668 edge boundary shows irregular near-circular shapes, given a
 669 more realistic path-loss exponent, which cannot be modeled
 670 accurately by either hexagonal or Voronoi topology.

REFERENCES

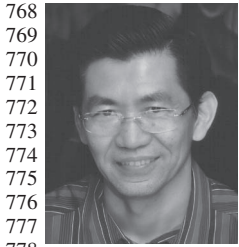
671
 672 [1] A. Damnjanovic *et al.*, "A survey on 3GPP heterogeneous networks,"
 673 *IEEE Wireless Commun.*, vol. 18, no. 3, pp. 10–21, Jun. 2011.
 674 [2] J. G. Andrews, "Seven ways that hetnets are a cellular paradigm shift,"
 675 *IEEE Commun. Mag.*, vol. 51, no. 3, pp. 136–144, Mar. 2013.
 676 [3] A. Ghosh, *et al.*, "Heterogeneous cellular networks: From theory to
 677 practice," *IEEE Commun. Mag.*, vol. 50, no. 6, pp. 54–64, Jun. 2012.

[4] J. G. Andrews, H. Claussen, M. Dohler, S. Rangan, and M. C. Reed, 678
 "Femtocells: Past, present, and future," *IEEE J. Sel. Areas Commun.*, 679
 vol. 30, no. 3, pp. 497–508, Apr. 2012. 680
 [5] X. Yang and A. P. Petropulu, "Co-channel interference modeling and 681
 analysis in a Poisson field of interferers in wireless communications," 682
IEEE Trans. Signal Process., vol. 51, no. 1, pp. 64–76, Jan. 2003. 683
 [6] A. D. Wyner, "Shannon-theoretic approach to a Gaussian cellular 684
 multiple-access channel," *IEEE Trans. Inf. Theory*, vol. 40, no. 6, 685
 pp. 1713–1727, Nov. 1994. 686
 [7] S. Shamai and A. D. Wyner, "Information-theoretic considerations for 687
 symmetric, cellular, multiple-access fading channels, Part I," *IEEE Trans.* 688
Inf. Theory, vol. 43, no. 6, pp. 1877–1894, Nov. 1997. 689
 [8] S. Shamai and A. D. Wyner, "Information-theoretic considerations 690
 for symmetric, cellular, multiple-access fading channels, Part II," *IEEE* 691
Trans. Inf. Theory, vol. 43, no. 6, pp. 1895–1911, Nov. 1997. 692
 [9] J. Xu, J. Zhang, and J. G. Andrews, "On the accuracy of the Wyner 693
 model in cellular networks," *IEEE Trans. Wireless Commun.*, vol. 10, 694
 no. 9, pp. 3098–3109, Sep. 2011. 695
 [10] F. Baccelli, M. Klein, M. Lebourges, and S. Zuyev, "Stochastic 696
 geometry and architecture of communication networks," *Telecommun.* 697
Syst., vol. 7, no. 1–3, pp. 209–227, Jun. 1997. 698
 [11] T. X. Brown, "Cellular performance bounds via shotgun cellular 699
 systems," *IEEE J. Sel. Areas Commun.*, vol. 18, no. 11, pp. 2443–2455, 700
 Nov. 2000. 701
 [12] J. G. Andrews, F. Baccelli, and R. K. Ganti, "A tractable approach to 702
 coverage and rate in cellular networks," *IEEE Trans. Commun.*, vol. 59, 703
 no. 11, pp. 3122–3134, Nov. 2011. 704
 [13] R. W. Heath and M. Kountouris, "Modeling heterogeneous network 705
 interference," in *Proc. IEEE ITA*, San Diego, CA, USA, Feb. 5–10, 2012, 706
 pp. 17–22. 707
 [14] H. S. Dhillon, R. K. Ganti, F. Baccelli, and J. G. Andrews, "Modeling 708
 and analysis of K-tier downlink heterogeneous cellular networks," *IEEE* 709
J. Sel. Areas Commun., vol. 30, no. 3, pp. 550–560, Apr. 2012. 710
 [15] M. Z. Win, P. C. Pinto, and L. A. Shepp, "A mathematical theory 711
 of network interference and its applications," *Proc. IEEE*, vol. 97, no. 2, 712
 pp. 205–230, Feb. 2009. 713
 [16] A. Busson and G. Chelius, "Point processes for interference modeling 714
 in CSMA/CA ad-hoc networks," in *Proc. 6th ACM Symp. Performance* 715
Eval. Wireless Ad Hoc, Sens., Ubiquitous Netw., Tenerife, Canary Islands, 716
 Spain, Oct. 26–30, 2009, pp. 33–40. 717
 [17] F. Baccelli, B. Błaszczyszyn, and P. Mühlethaler, "An Aloha protocol 718
 for multihop mobile wireless networks," *IEEE Trans. Inf. Theory*, vol. 52, 719
 no. 2, pp. 421–436, Feb. 2006. 720
 [18] H. Q. Nguyen, F. Baccelli, and D. Kofman, "A stochastic geometry 721
 analysis of dense IEEE 802.11 networks," in *Proc. 26th IEEE INFOCOM*, 722
 Anchorage, AK, USA, May 6–12, 2007, pp. 1199–1207. 723
 [19] M. L. Huber and R. L. Wolpert, "Likelihood-based inference for Matérn 724
 type-III repulsive point processes," *Adv. Appl. Probab.*, vol. 41, no. 4, 725
 pp. 958–977, Dec. 2009. 726
 [20] M. Haenggi, "Mean interference in hard-core wireless networks," *IEEE* 727
Commun. Lett., vol. 15, no. 8, pp. 792–794, Aug. 2011. 728
 [21] A. Hasan and J. G. Andrews, "The guard zone in wireless ad hoc 729
 networks," *IEEE Trans. Wireless Commun.*, vol. 6, no. 3, pp. 897–906, 730
 Mar. 2007. 731
 [22] B. Cho, K. Koufos, and R. Jantti, "Bounding the mean interference 732
 in Matérn type II hard-core wireless networks," *IEEE Wireless Commun.* 733
Lett., vol. 2, no. 5, pp. 563–566, Oct. 2013. 734
 [23] F. Jarai-Szabo and Z. Neda, "On the size-distribution of Poisson 735
 Voronoi cells," *Phys. A, Statist. Mech. Appl.*, vol. 385, no. 2, pp. 518–526, 736
 Feb. 2007. 737
 [24] D. Cao, S. Zhou, and Z. Niu, "Optimal combination of base station 738
 densities for energy-efficient two-tier heterogeneous cellular net- 739
 works," *IEEE Trans. Wireless Commun.*, vol. 12, no. 9, pp. 4350–4362, 740
 Sep. 2013. 741
 [25] S. Lee and K. Huang, "Coverage and economy of cellular networks with 742
 many base stations," *IEEE Commun. Lett.*, vol. 16, no. 7, pp. 1038–1040, 743
 Jul. 2012. 744
 [26] J.-M. Kelif, M. Coupechoux, and P. Godlewski, "A fluid model for per- 745
 formance analysis in cellular networks," *EURASIP J. Wireless Commun.* 746
Netw., vol. 2010, pp. 1–11, Aug. 2010. 747
 [27] F. Baccelli and B. Błaszczyszyn, *Stochastic Geometry and Wireless* 748
Networks, Volume I: Theory. Hanover, MA, USA: Now, 2009. 749
 [28] M. Haenggi, *Stochastic Geometry for Wireless Networks*. Cambridge, 750
 U.K.: Cambridge Univ. Press, 2013. 751
 [29] M. Kuczma, *An Introduction to the Theory of Functional Equations* 752
and Inequalities: Cauchy's Equation and Jensen's Inequality. Basel, 753
 Switzerland: Birkhauser, 2008. 754



Hui Zhang received the B.Eng. degree in applied mathematics and the Ph.D. degree in electrical engineering from Beijing University of Posts and Telecommunications, Beijing, China, in 2005 and 2010, respectively.

Since 2010, he has been a faculty member with the School of Electrical Information and Optical Engineering, Nankai University, Nankai, China. From 2013 to 2014, he was a Postdoctoral Scholar with the School of Electrical and Computer Science, University of Southampton, Southampton, U.K. In 2014, he joined in the China–Korea Young Scientist Exchange Program. His research interests include cellular networks and wireless communication theory.



Sheng Chen (M'90–SM'97–F'08) received the B.Eng. degree in control engineering from the East China Petroleum Institute, Dongying, China, in 1982; the Ph.D. degree in control engineering from the City University London, London, U.K., in 1986; and the D.Sc. degree from the University of Southampton, Southampton, U.K., in 2005.

From 1986 to 1999, he held research and academic appointments with The University of Sheffield, Sheffield, U.K.; The University of Edinburgh, Edinburgh, U.K.; and the University of Portsmouth, Portsmouth, U.K. Since 1999, he has been with Electronics and Computer Science, the University of Southampton, Southampton, U.K., where he is currently a Professor of intelligent systems and signal processing. He is also a Distinguished Adjunct Professor with King Abdulaziz University, Jeddah, Saudi Arabia. He is the author of over 500 research papers. His research interests include adaptive signal processing, wireless communications, modeling and identification of nonlinear systems, neural network and machine learning, intelligent control system design, and evolutionary computation methods and optimization.

779 Dr. Chen is a Fellow of the Institution of Engineering and Technology and
780 an ISI highly cited researcher in engineering (March 2004). In 2014, he was
781 elected as a Fellow of the United Kingdom Royal Academy of Engineering.



Liang Feng received the B.Eng. degree in applied physics from Dalian University of Technology, Dalian, China, in 2004. He is currently working toward the Master's degree with Nankai University, Nankai, China, in 2012.

From 2004 to 2012, he carried out electronic countermeasures research with the Luoyang Electronic Equipment Center, China. His research interests include cellular mobile communications.



Yifeng Xie received the B.S. degree in electronic and information engineering from Nanjing Forestry University, Nanjing, China, in 2011 and the M.S. degree in communication and information systems from Nankai University, Nankai, China, in 2014.

His research interests include stochastic geometry and heterogeneous networks.



Lajos Hanzo (F'08) received the Master's and D.Sc. degrees in electronics and the Doctor Honoris Causa from the Technical University of Budapest, Budapest, Hungary, in 1976 and 1983, respectively.

During his 38-year career in telecommunications, he has held various research and academic posts in Hungary, Germany, and the U.K. Since 1986, he has been with the School of Electronics and Computer Science, University of Southampton, Southampton, U.K., where he is the Chair in telecommunications.

He has successfully supervised about 100 Ph.D. students. He is the author or coauthor of 20 John Wiley/IEEE Press books on mobile radio communications, totalling in excess of 10 000 pages, and of more than 1400 research entries on IEEE Xplore. Currently, he is directing a 100-strong academic research team, working on a range of research projects in the field of wireless multimedia communications sponsored by industry, the Engineering and Physical Sciences Research Council (EPSRC) U.K., the European Research Council's Advanced Fellow Grant, and the Royal Society's Wolfson Research Merit Award. He is an enthusiastic supporter of industrial and academic liaison, and he offers a range of industrial courses.

Dr. Hanzo has acted both as a Technical Program Committee Chair and as a General Chair of IEEE conferences, has presented keynote lectures, and has received a number of distinctions. He is a Governor of the IEEE Vehicular Technology Society. From 2008 to 2012, he was the Editor-in-Chief of the IEEE Press and a Chaired Professor with Tsinghua University, Beijing, China. His research is funded by the European Research Council's Senior Research Fellow Grant. He is a Fellow of the Royal Academy of Engineering, the Institution of Engineering and Technology, and the European Association for Research and Signal Processing.

AUTHOR QUERIES

AUTHOR PLEASE ANSWER ALL QUERIES

AQ1 = Note that Ref. [7] was split into two. Consequently, the reference list and bibliographic citations were renumbered. Please check.

END OF ALL QUERIES

A Universal Approach to Coverage Probability and Throughput Analysis for Cellular Networks

Hui Zhang, Sheng Chen, *Fellow, IEEE*, Liang Feng, Yifeng Xie, and Lajos Hanzo, *Fellow, IEEE*

Abstract—This paper proposes a novel tractable approach for accurately analyzing both the coverage probability and the achievable throughput of cellular networks. Specifically, we derive a new procedure referred to as the equivalent uniform-density plane-entity (EUDPE) method for evaluating the other-cell interference. Furthermore, we demonstrate that our EUDPE method provides a universal and effective means to carry out the lower bound analysis of both the coverage probability and the average throughput for various base-station distribution models that can be found in practice, including the stochastic Poisson point process (PPP) model, a uniformly and randomly distributed model, and a deterministic grid-based model. The lower bounds of coverage probability and average throughput calculated by our proposed method agree with the simulated coverage probability and average throughput results and those obtained by the existing PPP-based analysis, if not better. Moreover, based on our new definition of cell edge boundary, we show that the cellular topology with randomly distributed base stations (BSs) only tends toward the Voronoi tessellation when the path-loss exponent is sufficiently high, which reveals the limitation of this popular network topology.

Index Terms—Achievable throughput, cellular coverage, cellular networks, deterministic grid-based model, Poisson point process (PPP) model, uniformly and randomly distributed model.

I. INTRODUCTION

SINCE cellular systems are under growing pressure to increase the volume of data delivered to consumers, establishing an accurate performance prediction model is of prime significance [1]. Cellular systems are evolving into a large-scale heterogeneous network architecture, constructed by overlapping network tiers, such as macrocells, picocells, femtocells, etc. [2]–[4]. The traditional cellular analysis relying on an idealized hexagonal model does not realistically represent the actual distribution of cells. Clearly, such a simplistic model

cannot be used for accurately modeling real-world cellular networks and for analyzing the coverage probability and the achievable throughput. Two mathematical models, i.e., the cellular system interference model and the base station (BS) or cell distribution model, are fundamental in the coverage analysis.

A. Related Work and Motivation

According to [5], the interference models can generally be divided into two types: empirical models and statistical–physical models. The construction of an empirical interference model relies on first measuring the interference and then fitting a mathematical model to the data. By contrast, the derivation of a statistical–physical model usually relies on the mathematical modeling of the interference. The classic Wyner model [6] was proposed in 1994, and since then, it has been widely adopted in the analysis of cellular networks. This model assumes that the interference is constituted by the sum of the signals transmitted from the adjacent cells (typically only considering two neighbors), which is often multiplied by a fixed scaling factor or gain to represent the specific intensity of the interferers [6]–[9].

Determining the most beneficial positions of the BSs represents a critical planning problem in cellular networks. Traditional methods usually place the BSs deterministically on a regular grid, despite the fact that, in practice, the positions of BSs are influenced by many random factors. Taking into account the randomness of BS locations, in [10] and [11], a stochastic-geometry-based method for modeling the positions of the BSs was derived, whereas in [12] and [13], it was proposed that the BSs be placed according to a homogeneous Poisson point process (PPP) associated with a given intensity [12], [13]. However, since the cellular network is gradually evolving into a large-scale heterogeneous network associated with multiple-tier random BS locations, the design challenge becomes more grave. A recent contribution [14] has demonstrated that the BS locations may be drawn from a PPP, particularly for single-tier networks. In [5], the statistical–physical modeling of cochannel interference (CCI) was investigated by assuming that the geographic distribution of interferers is known *a priori* and that the interferers belong to a Poisson field, with each individual interferer having a random session life time. In [15], a mathematical theory based on a spatially homogeneous PPP was provided to analyze the effects of interference, which models the spatial distribution of the nodes over the 2-D infinite plane by PPP theory.

The PPP model was used in [12] for establishing a heterogeneous network model of a single-tier macrocell network.

Manuscript received March 5, 2014; revised August 31, 2014; accepted October 28, 2014. This work was supported in part by the National Natural Science Foundation Project of China under Grant 61101084 and in part by the Fundamental Research Funds for the Central Universities, China. The review of this paper was coordinated by Dr. Y. Ma.

H. Zhang, L. Feng, and Y. Xie are with the Wireless Communications Laboratory, Information College, Nankai University, Tianjin 300071, China (e-mail: zhangh@nankai.edu.cn; fengliang201203@gmail.com; xyfhope@gmail.com).

S. Chen is with the School of Electronics and Computer Science, University of Southampton, Southampton SO17 1BJ, U.K., and also with King Abdulaziz University, Jeddah 21589, Saudi Arabia (e-mail: sqc@ecs.soton.ac.uk).

L. Hanzo is with School of Electronics and Computer Science, University of Southampton, Southampton SO17 1BJ, U.K. (e-mail: lh@ecs.soton.ac.uk).

Color versions of one or more of the figures in this paper are available online at <http://ieeexplore.ieee.org>.

Digital Object Identifier 10.1109/TVT.2014.2366597

84 Based on this PPP model, the calculation of the cumulative
 85 interference imposed by all surrounding BSs can be carried
 86 out with the aid of the Laplace transform and the probability
 87 generating function [12], [14]. Furthermore, the coverage prob-
 88 ability expression was deduced for the specific scenario, when
 89 the interference experiences Rayleigh fading, and the results
 90 of [12] and [14] demonstrated that the analysis based on the
 91 PPP-aided modeling represent the lower bound of simulation
 92 results.¹ Similarly, the achievable average rate was also calcu-
 93 lated. Although the PPP model is adopted for the analysis of
 94 cellular networks, it is only accurate for sparse networks. By
 95 contrast, it suffers from a lack of realism in the case of dense
 96 networks since it may place several BSs far too closely together,
 97 which does not make practical sense as such a situation will not
 98 occur in a real BS deployment. It may impose excessive CCI if
 99 too many BSs are deployed too densely. Noting this weakness
 100 of the PPP model, some balanced measures are suggested to
 101 alleviate this drawback in [12], but this weakness cannot be fun-
 102 damentally eliminated by these measures. Moreover, the PPP-
 103 based analysis relies on the assumption that the transmitters are
 104 independently distributed [16].

105 A range of alternative stochastic-geometry-based methods
 106 have also been used in the analysis of wireless networks [17],
 107 [18]. For example, in [17], the Matérn hard-core process was
 108 invoked for modeling the classic carrier sense multiple access
 109 (CSMA) protocol and for analyzing its throughput, where the
 110 presence of interferers within a given radius around any trans-
 111 mitter was prevented. The Matérn point process [19] was modi-
 112 fied in [18] to model the CSMA with collision avoidance, which
 113 yields more realistic results by applying the aforementioned
 114 interference-exclusion zone around all possible transmitters.
 115 However, coverage analysis based on a Matérn hard-core pro-
 116 cess is difficult to carry out [20] since the probability generating
 117 functional of a Matérn hard-core process does not exist. It was
 118 argued in [20]–[22] that only the Matérn type II process causes
 119 a level of interference comparable to that predicted by a PPP
 120 and, therefore, for interference-based performance analysis, the
 121 Matérn type II process may be safely approximated by the
 122 corresponding nonhomogeneous PPP [20]–[22].

123 B. Our Approach and Contributions

124 Against the above background, we propose a novel universal
 125 approach for tractable and accurate coverage analysis of cellu-
 126 lar networks. Our contributions are as follows.

127 1) *Physical Analysis of Hexagonal/Voronoi Cells:* To inter-
 128 pret the various geometric-based cellular models from a phys-
 129 ical perspective, we provide a tangible generic definition of the
 130 cell edge boundary for our theoretical analysis, where the cell
 131 boundary is directly linked to the path-loss exponent. Specif-
 132 ically, we show that the traditional hexagonal topology natu-
 133 rally emerges from the grid-based model, given a sufficiently
 134 high path-loss exponent, whereas the Voronoi tessellation nat-
 135 urally emerges from the random BS distribution model, again

provided that the path-loss exponent is sufficiently high. How- 136
 ever, such a high path-loss exponent is unrealistic in real trans- 137
 mission environments. Therefore, our physical analysis reveals 138
 the fundamental limitation of these purely graphic-based cellu- 139
 lar topologies, namely, lack of the connection to the underlying 140
 signal transmission medium. In fact, we demonstrate that the 141
 cell edge boundary shows irregular near-circular shapes, given a 142
 more realistic path-loss exponent of around 3, which cannot be 143
 modeled accurately by either hexagonal or Voronoi tessellation. 144

2) *EUDPE-Based Other-Cell Interference Model:* We pro- 145
 pose a universal model for evaluating the other-cell interfer- 146
 ence, which we refer to as the equivalent uniform-density 147
 plane-entity (EUDPE) method. This generic EUDPE model can 148
 be used to calculate the cumulative other-cell interference for 149
 all the existing BS distribution models that can be found in 150
 practice, including both stochastic and deterministic cellular 151
 network models, such as the stochastic Poisson distributed (PD) 152
 and uniformly distributed (UD) BS models and the determinis- 153
 tic grid-based BS model. 154

3) *Lower Bound Analysis for Coverage Probability and* 155
Average Achievable Rate: Based on the proposed generic 156
 EUDPE interference model, we perform the low-bound anal- 157
 ysis of both the coverage probability and the average achiev- 158
 able rate for various BS distribution models, specifically, the 159
 stochastic PD and UD BS models and the deterministic grid- 160
 based BS model, which may be viewed as a degenerated or spe- 161
 cial case of the UD BS model. For realistic path-loss exponents, 162
 the coverage probability and average achievable throughput 163
 results provided by our proposed analysis approach agree with 164
 the simulated coverage probability and achievable throughput. 165
 In fact, their match is as good or better than that of the PPP- 166
 based analysis. The results also show that the noise only has a 167
 modest effect on the coverage probability and achievable rate. 168

The remainder of this paper is organized as follows. In 169
 Section II, the downlink cellular system model is briefly in- 170
 troduced, which is followed by our new physical analysis of 171
 cell edge boundary. Section III is devoted to the derivation of 172
 our EUDPE-based interference model. The low-bound analysis 173
 of the coverage probability based on the EUDPE method is 174
 deduced in Section IV for both stochastic BS distribution 175
 models and deterministic grid-based BS models, whereas the 176
 corresponding low-bound analysis is presented in Section V. 177
 Our conclusions are offered in Section VI. 178

179 II. DOWNLINK CELLULAR SYSTEM MODEL

Throughout our discussions, the index set of the BSs, which 180
 are deployed according to some distribution, is denoted by Φ , 181
 whereas the serving BS's index is denoted by b_0 . Furthermore, 182
 the average density of BSs is ρ . Let P be the transmitted power 183
 of a BS, R be the serving BS's coverage radius, R_{nw} be the 184
 distance from the serving BS to the edge of the network, and 185
 r_i denotes the distance from the i th BS to the user equipment 186
 (UE) concerned. If we denote the average coverage area of a 187
 BS by $\mathbb{E}[A_s]$ with $\mathbb{E}[\cdot]$ representing the expectation operator, 188
 then $\mathbb{E}[A_s] = 1/\rho$. We will also use $2R$ to denote the average 189
 distance between two neighboring BSs, and we have $R \propto$ 190
 $\sqrt{\mathbb{E}[A_s]}$. 191

¹The simulation results are referred to as "experimental" or "actual" in [12], which is inappropriate.

192 A. SINR Model

193 The wireless channel linking the i th BS and the UE con-
 194 sidered is modeled by a complex-valued channel tap that takes
 195 into account the path loss with a path-loss exponent of α , the
 196 fast Rayleigh fading coefficient with an instantaneous power
 197 or a squared magnitude of h_i , and the channel's additive white
 198 Gaussian noise (AWGN) with noise power of σ^2 . The average
 199 of the random variable h_i is denoted by \bar{h} ; therefore, h_i follows
 200 the exponential distribution with the mean \bar{h} .

201 Let us assume that the intracell UE-to-UE interference is neg-
 202 ligible. Then, the signal-to-interference-plus-noise ratio (SINR)
 203 experienced at this UE can be expressed as follows:

$$\text{SINR} = \frac{Ph_0r_0^{-\alpha}}{I_r + \sigma^2} \quad (1)$$

204 where the interference arriving from all the interfering cells is
 205 given by

$$I_r = \sum_{i \in \Phi \setminus b_0} Ph_i r_i^{-\alpha}. \quad (2)$$

206 If the target SINR value is T , then the actual SINR must obey
 207 $\text{SINR} > T$, which requires

$$h_0 > P^{-1}Tr_0^\alpha (\sigma^2 + I_r). \quad (3)$$

208 Thus, the probability distribution of h_0 should be taken into
 209 account in the analysis of both the coverage probability and the
 210 average rate. Furthermore, intuitively, the given SINR model
 211 determines the coverage area of each BS; therefore, it influences
 212 the cell shape or boundary.

213 B. Physical Analysis of Cell Edge Boundary

214 As aforementioned, the grid-based cellular model is conve-
 215 nient but is too idealistic. By contrast, the Voronoi tessellation is
 216 considered to match the random BS deployment in relative flat
 217 urban areas reasonably well [12], [23]. Hence, cellular networks
 218 can be analyzed using Voronoi diagram theory, albeit this has
 219 not been explained with the aid of a physically tangible per-
 220 spective. More specifically, both the energy efficiency and cov-
 221 erage of cellular networks may be analyzed based on Voronoi
 222 tessellation [24], [25]. Fig. 1 shows a random distribution of
 223 the BSs with the cell boundaries corresponding to a Voronoi
 224 tessellation. Note that in both the grid-based and Voronoi-based
 225 cellular topologies, the cell boundaries are determined purely
 226 by the geometric property of the BS distribution, and they are
 227 completely independent of the actual physical interference that
 228 the network is experiencing.

229 To interpret the cell edge boundary from a physical percep-
 230 tively, namely, linking it better to the underlying physics of
 231 signal transmission medium, let us now introduce the following
 232 definition that formally defines the cell edge boundary.

233 *Definition 1:* The cell edge boundary is constituted by the
 234 group of points where the strength of the desired signal received
 235 from the serving BS equals to the interfering signal's strength.
 236 In other words, at the cell edge boundary, the desired signal-
 237 to-interference ratio (SIR) is equal to 1. This definition of cell

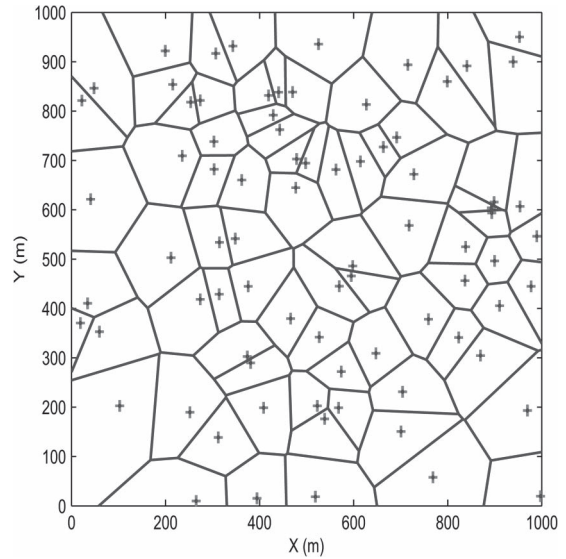


Fig. 1. Random distribution of the BSs marked by +, with the cell boundaries corresponding to a Voronoi tessellation.

edge boundary is both intuitive and practical since, within the
 238 coverage area of a BS, the desired signal should be stronger than
 239 the interfering signal, yielding $\text{SIR} > 1$. Let us denote the i th
 240 BS location as the point z_i , where $i \in \Phi$. Furthermore, denote
 241 the distance from z_i to a point z as $|z - z_i|$. The desired signal
 242 power at the point z provided by the i th BS is given by
 243

$$S(z) = \mathbb{E} [Ph_i |z - z_i|^{-\alpha}] = P\bar{h} |z - z_i|^{-\alpha} \quad (4)$$

while the interfering signal's power at z is given by
 244

$$\begin{aligned} I(z) &= \mathbb{E} [I_r(z)] = \mathbb{E} \left[\sum_{j \in \Phi \setminus i} Ph_j |z - z_j|^{-\alpha} \right] \\ &= P\bar{h} \sum_{j \in \Phi \setminus i} |z - z_j|^{-\alpha}. \end{aligned} \quad (5)$$

Thus, with respect to the i th BS, the SIR at the point z is 245
 given by
 246

$$\text{SIR}(z) = \frac{|z - z_i|^{-\alpha}}{\sum_{j \in \Phi \setminus i} |z - z_j|^{-\alpha}}. \quad (6)$$

Therefore, at the i th cell's edge boundary, we have $\text{SIR}(z) = 1$. 247

In Figs. 2 and 3, the distribution of the BSs is based on the
 248 same regular grid network model, and the number of BSs is 33. 249
 As shown in Fig. 2, the shape of each cell in the network is
 250 approximately a regular circle given the path-loss exponent of
 251 $\alpha = 3$. By contrast, observe in Fig. 3 that the cell shape changes
 252 into a hexagonal one when the path-loss exponent is increased
 253 to $\alpha = 10$.
 254

In Figs. 4 and 5, the locations of the 33 BSs are randomly
 255 drawn from the uniform distribution across the entire network
 256 area. The cells now approximately have irregularly circular
 257 shapes when the path-loss exponent is $\alpha = 3$, but interestingly,
 258 it is the Voronoi tessellation that naturally emerges when the
 259 path-loss exponent is increased to $\alpha = 10$.
 260

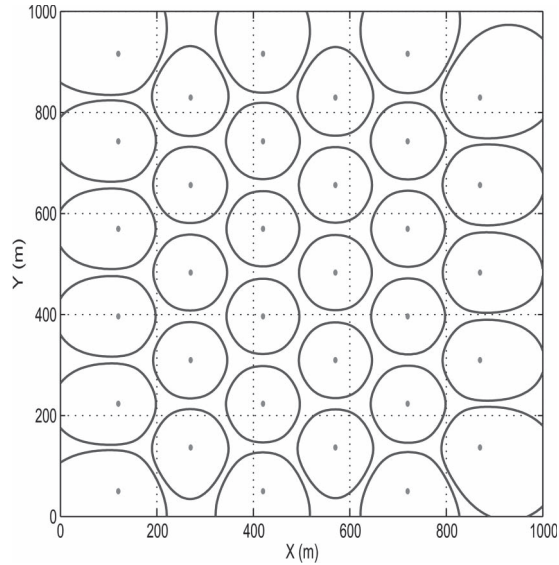


Fig. 2. Cell edge boundaries of the grid network model with the 33 BS locations marked by dots, as determined by $SIR(z) = 1$. The path-loss exponent is $\alpha = 3$.

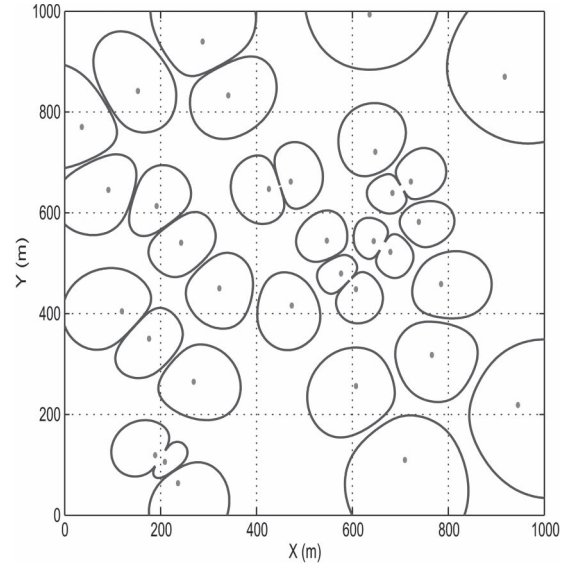


Fig. 4. Cell edge boundaries of the randomly distributed network model with the 33 BS locations marked by dots, as determined by $SIR(z) = 1$. The path-loss exponent is $\alpha = 3$.

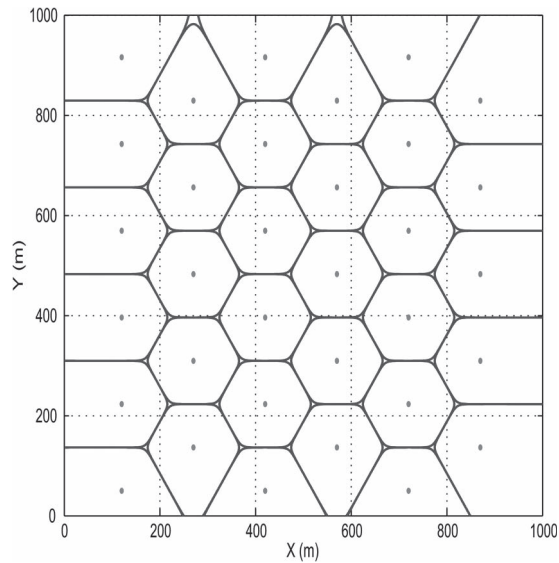


Fig. 3. Cell edge boundaries of the grid network model with the 33 BS locations marked by dots, as determined by $SIR(z) = 1$. The path-loss exponent is $\alpha = 10$.

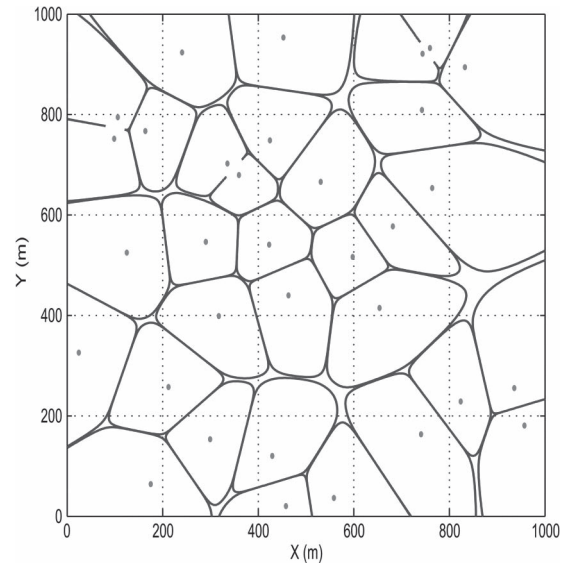


Fig. 5. Cell edge boundaries of the randomly distributed network model with the 33 BS locations marked by dots, as determined by $SIR(z) = 1$. The path-loss exponent is $\alpha = 10$.

261 The given results demonstrate that our Definition 1 of cell
 262 edge boundary is a physically plausible one for analyzing the
 263 network, and both the hexagonal topology and the Voronoi
 264 tessellation naturally emerge according to this definition, de-
 265 pending on whether the geographic distribution of BSs is deter-
 266 ministic or random and providing that the path-loss exponent
 267 is sufficiently high. Note that such a high path-loss exponent
 268 is unrealistic in real transmission environments. Therefore,
 269 our analysis of cell edge boundary reveals a weakness of the
 270 popular hexagonal and Voronoi network topologies, namely,
 271 they do not reflect the underlying signal transmission medium.
 272 Significantly, given a more realistic path-loss exponent of ap-
 273 proximately three, the cell edge boundary exhibits irregular

near-circular cell shapes, for which neither hexagonal topology 274
 nor Voronoi tessellation can be used to accurately model. 275
 Furthermore, the “weak” coverage areas that are left outside 276
 any cell boundary, where the desired signal is weaker than the 277
 interfering signals, as shown in Fig. 4, highlight the benefits of 278
 employing collaborative relaying techniques. 279

III. EQUIVALENT UNIFORM DENSITY PLANE-ENTITY FOR 280 CUMULATIVE INTERFERENCE CALCULATION 281

To accurately analyze the coverage probability and the 282
 achievable rate, it is necessary to find an efficient means for 283

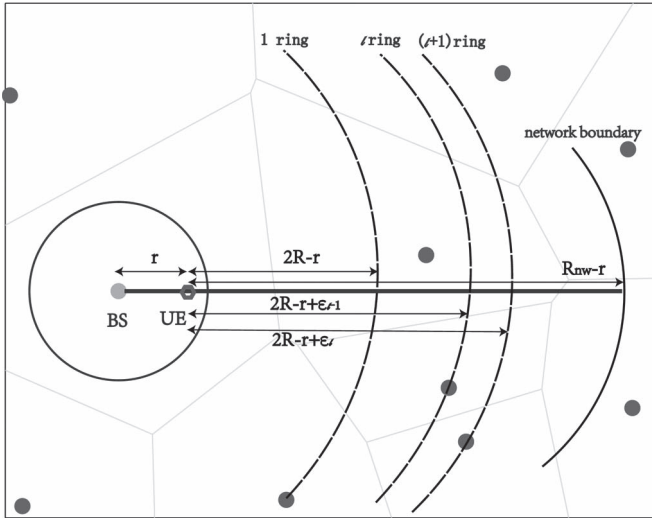


Fig. 6. Proposed EUDPE method for calculating the other-cell interference.

284 cumulative interference calculation. By considering the dis-
 285 tribution of the interference imposed by the BSs in the law
 286 of large numbers and combining it with the fluid model of
 287 [26], we propose the EUDPE method for calculating the cu-
 288 mulative interference. The basic idea of this EDUPE method
 289 is as follows. Although the actual geographic distribution of
 290 BSs always shows a certain degree of irregularity, we may
 291 define a group of equivalent and uniformly distributed BSs for
 292 approximating the other-cell CCI. Since, in real-world cellular
 293 networks, the actual geographic distribution of BSs is often
 294 close to a uniform random distribution, such an approximation
 295 is sufficiently accurate. It is worth emphasizing however that
 296 we do not assume a uniform and random BS distribution for
 297 the actual network to be modeled. More specifically, given
 298 a network having the average BS density of ρ , we approx-
 299 imate this network with an equivalent network whose BSs
 300 are uniformly distributed and whose BS density is also ρ .
 301 Such a network is termed the equivalent EUDPE of the given
 302 network. With the aid of our EUDPE method, we can calcu-
 303 late or approximate the cumulative interference for any given
 304 network.

305 Fig. 6 illustrates the concept of the EUDPE, where the
 306 serving BS is assumed the origin of the polar coordinate plane.
 307 Since the coverage radius of a BS is R , the distance between
 308 two neighboring BSs is $2R$, where $R \propto (1/\sqrt{\rho})$. For notational
 309 simplification, we drop the subscript 0 from r_0 and denote the
 310 distance from the serving BS to the UE as r , where $0 \leq r \leq R$.
 311 Thus, the distance from the nearest interfering BS to the UE
 312 is $(2R - r)$. As shown in Fig. 6, the network's coverage area
 313 is partitioned by the N_r rings, and the distance from the UE
 314 to the l th ring is given by $(2R - r + \varepsilon_{l-1})$, where $1 \leq l \leq$
 315 N_r with $\varepsilon_0 = 0$ and $(2R - r + \varepsilon_{N_r}) = R_{nw} - r$. The number
 316 of BSs within the area between the l th and $(l + 1)$ th rings
 317 is approximately $\int_0^{2\pi} \int_{2R-r+\varepsilon_{l-1}}^{2R-r+\varepsilon_l} \rho z dz d\theta$ when assuming the
 318 equivalent EUDPE having the BS density of ρ . Furthermore,
 319 each of these equivalent BSs has the same instantaneous
 320 fast fading channel power of \tilde{h}_l , and the mean of \tilde{h}_l is \bar{h} .

Thus, the cumulative interference I_r can be approximated 321
 according to 322

$$\begin{aligned} I_r &= \sum_{l=1}^{N_r} \int_0^{2\pi} \int_{2R-r+\varepsilon_{l-1}}^{2R-r+\varepsilon_l} P\tilde{h}_l z^{-\alpha} \rho z dz d\theta \\ &= \sum_{l=1}^{N_r} \frac{2\pi\rho P\tilde{h}_l}{\alpha-2} \left((2R-r+\varepsilon_{l-1})^{2-\alpha} - (2R-r+\varepsilon_l)^{2-\alpha} \right). \end{aligned} \quad (7)$$

Theorem 1: The average of I_r is given by 323

$$\mathbb{E}[I_r] = \frac{2\pi\rho P\bar{h}}{\alpha-2} \left((2R-r)^{2-\alpha} - (R_{nw}-r)^{2-\alpha} \right). \quad (8)$$

Proof: According to the Campbell-Mecke theorem [27], 324
 we have 325

$$\begin{aligned} \mathbb{E} \left[\sum_{l=1}^{N_r} \frac{2\pi\rho P\tilde{h}_l}{\alpha-2} \left((2R-r+\varepsilon_{l-1})^{2-\alpha} - (2R-r+\varepsilon_l)^{2-\alpha} \right) \right] \\ = \sum_{l=1}^{N_r} \frac{2\pi\rho P\mathbb{E}[\tilde{h}_l]}{\alpha-2} \left((2R-r+\varepsilon_{l-1})^{2-\alpha} - (2R-r+\varepsilon_l)^{2-\alpha} \right) \\ = \frac{2\pi\rho P\bar{h}}{\alpha-2} \left((2R-r)^{2-\alpha} - (R_{nw}-r)^{2-\alpha} \right). \end{aligned} \quad (9)$$

326

Typically, the path-loss exponent is $\alpha > 2$ in realistic net- 327
 works. Noting that $(R_{nw}-r)^{2-\alpha} \rightarrow 0$ as $R_{nw} \rightarrow +\infty$, we 328
 have the following corollary. 329

Corollary 1: Given that the network's boundary is suffi- 330
 ciently far away, namely, $R_{nw} \rightarrow +\infty$, we have 331

$$\mathbb{E}[I_r] = \frac{2\pi\rho P\bar{h}}{\alpha-2} (2R-r)^{2-\alpha}. \quad (10)$$

IV. COVERAGE PROBABILITY ANALYSIS USING 332 EQUIVALENT UNIFORM DENSITY PLANE-ENTITY 333

As mentioned earlier, the cellular system interference model 334
 and the BS geographic distribution model are required in cov- 335
 erage analysis. Our proposed EUDPE is a universal method 336
 for evaluating the other-cell interference for all existing BS 337
 distribution models, such as the stochastic PD and UD BS 338
 models and the deterministic grid-based model. 339

A. Coverage Probability Analysis Using EUDPE-PD 340

Since a popular geographic BS distribution is the Poisson 341
 distribution [12]–[15], we first consider the PD BS model. The 342
 probability density function (pdf) of the Poisson distribution 343
 can be derived using the method of [28]. Let λ be the intensity 344
 of the Poisson distribution that models the BS geographic 345
 distribution and R be the average coverage radius of a cell. 346
 Then, the probability of having no BS that is closer than x is 347
 given by 348

$$\mathbb{P}\{r > x\} = \mathbb{P}\{\text{No BS closer than } x\} = e^{-\lambda\pi x^2}. \quad (11)$$

349 The corresponding cumulative distribution function (cdf) is
350 then given by

$$\mathbb{P}\{r \leq x\} = F(x) = 1 - e^{-\lambda\pi x^2}. \quad (12)$$

351 Therefore, the pdf is defined as

$$f(r) = \frac{dF(r)}{dr} = 2\pi\lambda r e^{-\pi\lambda r^2}. \quad (13)$$

352 Given the SINR threshold T , the intensity λ and the path-loss
353 exponent α , the coverage probability is defined as

$$\begin{aligned} p_c(T, \lambda, \alpha) &= \mathbb{E}_r [\mathbb{E}_{I_r} [\mathbb{P}\{\text{SINR} > T\}]] \\ &= \int_{r>0} \mathbb{E}_{I_r} [\mathbb{P}\{h_0 > P^{-1}Tr^\alpha(\sigma^2 + I_r)\}] 2\pi\lambda r e^{-\pi\lambda r^2} dr \end{aligned} \quad (14)$$

354 where $\mathbb{E}_r[\bullet]$ denotes the expectation with respect to the random
355 variable r .

356 1) *Lower Bound for the Probability of SINR Larger Than*
357 *Threshold:* Noting that h_0 obeys the exponential distribution
358 with the mean \bar{h} , the probability of the SINR larger than the
359 threshold T (averaged over the interference) is given by

$$\begin{aligned} \mathbb{E}_{I_r} [\mathbb{P}\{h_0 > P^{-1}Tr^\alpha(\sigma^2 + I_r)\}] \\ = e^{-\bar{h}P^{-1}Tr^\alpha\sigma^2} \mathbb{E}_{I_r} [e^{-\bar{h}P^{-1}Tr^\alpha I_r}]. \end{aligned} \quad (15)$$

360 *Theorem 2:* A lower bound for the probability of the SINR
361 greater than the threshold T is expressed as

$$\mathbb{E}_{I_r} [\mathbb{P}\{h_0 > P^{-1}Tr^\alpha(\sigma^2 + I_r)\}] \geq e^{-\bar{h}Tr^\alpha\eta(\alpha, r)} \quad (16)$$

362 where

$$\eta(\alpha, r) = P^{-1}\sigma^2 + \frac{2\pi\rho\bar{h}}{\alpha-2} ((2R-r)^{2-\alpha} - (R_{\text{nw}}-r)^{2-\alpha}). \quad (17)$$

363 *Proof:* According to Jensen's inequality [29], we have

$$\mathbb{E}_{I_r} [e^{-\bar{h}P^{-1}Tr^\alpha I_r}] \geq e^{-\bar{h}P^{-1}Tr^\alpha \mathbb{E}[I_r]}. \quad (18)$$

364 Substituting (18) into (15) and noting $\mathbb{E}[I_r]$ of (8) leads to (16)
365 with $\eta(\alpha, r)$ given in (17). ■

366 *Corollary 2:* Given that the network boundary is sufficiently
367 far away, namely, $R_{\text{nw}} \rightarrow +\infty$

$$\mathbb{E}_{I_r} [\mathbb{P}\{h_0 > P^{-1}Tr^\alpha(\sigma^2 + I_r)\}] \geq e^{-\bar{h}Tr^\alpha\xi(\alpha, r)} \quad (19)$$

368 where

$$\xi(\alpha, r) = P^{-1}\sigma^2 + \frac{2\pi\rho\bar{h}}{\alpha-2} (2R-r)^{2-\alpha}. \quad (20)$$

369 2) *Lower Bound for the Coverage Probability:* A lower
370 bound for the coverage probability $p_c(T, \lambda, \alpha)$ is given by the
371 following theorem.

Theorem 3: For the network where the BS geographic 372
distribution obeys the Poisson distribution of intensity λ , 373
a lower bound for the coverage probability $p_c(T, \lambda, \alpha)$ is 374
given by 375

$$p_{cl}(T, \lambda, \alpha) = \pi\lambda \int_0^{R^2} e^{-\bar{h}Tv^{\alpha/2}\psi(\alpha, v) - \pi\lambda v} dv \quad (21)$$

where R is the coverage radius of the serving BS, and 376

$$\begin{aligned} \psi(\alpha, v) &= P^{-1}\sigma^2 + \frac{2\pi\rho\bar{h}}{\alpha-2} \left((2R - v^{1/2})^{2-\alpha} \right. \\ &\quad \left. - (R_{\text{nw}} - v^{1/2})^{2-\alpha} \right). \end{aligned} \quad (22)$$

Proof: From (14) and Theorem 2, as well as noting that 377
 $r \leq R$, we have 378

$$p_{cl}(T, \lambda, \alpha) = \int_0^R 2\pi\lambda r e^{-\bar{h}Tr^\alpha\eta(\alpha, r) - \pi\lambda r^2} dr. \quad (23)$$

By defining $r^2 = v$, (23) is transformed into (21) with $\psi(\alpha, v)$ 379
given in (22). ■ 380

Corollary 3: Given that the network boundary is sufficiently 381
far away, namely, $R_{\text{nw}} \rightarrow +\infty$, a lower bound for the coverage 382
probability $p_c(T, \lambda, \alpha)$ is expressed as 383

$$p_{cl}(T, \lambda, \alpha) = \pi\lambda \int_0^{R^2} e^{-\bar{h}Tv^{\alpha/2}\chi(\alpha, v) - \pi\lambda v} dv \quad (24)$$

where 384

$$\chi(\alpha, v) = P^{-1}\sigma^2 + \frac{2\pi\rho\bar{h}}{\alpha-2} (2R - v^{1/2})^{2-\alpha}. \quad (25)$$

Remark 1: In the coverage analysis for the EUDPE-PD 385
model, the average coverage radius R is related to the average 386
cell area $\mathbb{E}[A_s]$. Noting $R \propto \sqrt{\mathbb{E}[A_s]}$ and $\mathbb{E}[A_s] = 1/\rho$, we 387
may use 388

$$R = \frac{c_f}{\sqrt{\rho}} \quad (26)$$

where c_f is an empirically chosen factor. For example, if the 389
average cell is defined by a square shape, we have $\mathbb{E}[A_s] = 390$
 $4R^2$; therefore, we have $c_f = 1/2 = 0.5$. On the other hand, 391
if the average coverage area is calculated according to a hexag- 392
onal one, we have $\mathbb{E}[A_s] = 2\sqrt{3}R^2$, yielding $c_f = 1/\sqrt{2\sqrt{3}} \approx 393$
 0.54 , whereas for the average circle-shape cell, we have $c_f = 394$
 $1/\sqrt{\pi} \approx 0.56$. 395

B. Coverage Probability Analysis Using EUDPE-UD 396

For many practical cellular networks, the geographic BS 397
distribution is often close to a uniform random distribution. 398
Therefore, we next consider the UD BS model with the average 399

400 density of BSs given by ρ . In this case, the corresponding cdf is
401 given by

$$\mathbb{P}\{z \leq x\} = F(x) = \frac{x^2}{c_{\text{nm}}^2} \rho, \quad 0 \leq x \leq R \quad (27)$$

402 where c_{nm}^2 is a normalization factor, and R is the coverage
403 radius of the serving BS. Thus, the pdf is given as

$$f(r) = \frac{2\rho}{c_{\text{nm}}^2} r, \quad 0 \leq r \leq R. \quad (28)$$

404 The normalization factor c_{nm}^2 is determined as follows. Assume
405 that $E[A_s] = R^2/c_f^2$, where c_f is defined in (26), and fur-
406 ther note that $E[A_s] = 1/\rho$. From $\int_0^R f(r) dr = 1$, we obtain
407 $c_{\text{nm}}^2 = c_f^2$.

408 The coverage probability is therefore defined as

$$\begin{aligned} p_c(T, \rho, \alpha) &= \mathbb{E}_r [\mathbb{E}_{I_r} [\mathbb{P}\{\text{SINR} > T\}]] \\ &= \frac{\rho}{c_f^2} \int_0^R \mathbb{E}_{I_r} [\mathbb{P}\{h_0 > P^{-1} T r^\alpha (\sigma^2 + I_r)\}] 2r dr. \end{aligned} \quad (29)$$

409 A lower bound of $\mathbb{E}_{I_r} [\mathbb{P}\{h_0 > P^{-1} T r^\alpha (\sigma^2 + I_r)\}]$ is given in
410 Theorem 2. Similar to the case of the EUDPE-PD expressed in
411 Theorem 3, therefore, a lower bound for the coverage probabil-
412 ity $p_c(T, \rho, \alpha)$ is given by the following theorem.

413 *Theorem 4:* For the network where the BS geographic distri-
414 bution obeys the uniform random distribution with an average
415 BS density of ρ , a lower bound for the coverage probability
416 $p_c(T, \rho, \alpha)$ is given by

$$p_{cl}(T, \rho, \alpha) = \frac{\rho}{c_f^2} \int_0^{R^2} e^{-\bar{h} T v^{\alpha/2} \psi(\alpha, v)} dv \quad (30)$$

417 where $\psi(\alpha, v)$ is defined in (22).

418 *Corollary 4:* Given that the network boundary is sufficiently
419 far away, a lower bound for the coverage probability $p_c(T, \rho, \alpha)$
420 is expressed by

$$p_{cl}(T, \rho, \alpha) = \frac{\rho}{c_f^2} \int_0^{R^2} e^{-\bar{h} T v^{\alpha/2} \chi(\alpha, v)} dv \quad (31)$$

421 where $\chi(\alpha, v)$ is defined in (25).

422 *Remark 2:* How to set the average coverage radius R is
423 explained in Remark 1. Specifically, we may use $R = c_f/\sqrt{\rho}$,
424 where c_f is an empirically chosen factor.

425 C. Coverage Probability Analysis Using EUDPE-Grid

426 With the aid of the EUDPE method, it is straightforward to
427 carry out the coverage probability analysis for all the traditional
428 deterministic grid-based cellular network models, such as the
429 squared and hexagonal ones. This is because the coverage
430 probability analysis using the EUDPE-Grid model is simply a
431 degenerated or special case of the EUDPE-UD-based analysis,

where the density of BSs ρ is identical everywhere in the net- 432
work, and every cell has the identical shape with the same area 433
 A_s . Therefore, the lower bounds of the coverage probability for 434
the finite-size and infinite-size grid-based network models are 435
given in Theorem 4 and Corollary 4, respectively. Moreover, 436
choosing $R = 1/(2\sqrt{\rho})$ corresponds to the grid-based network 437
with squared cells, whereas using $R = 1/(\sqrt{2\sqrt{3}}\sqrt{\rho})$ is related 438
to considering the grid-based network with hexagonal cells. In 439
general, we may use $R = c_f/\sqrt{\rho}$ for any deterministic grid- 440
based network by choosing an appropriate value for c_f . It be- 441
comes obvious that, under the equivalent network environment 442
of the same ρ and R values, the coverage probability obtained 443
by the EUDPE-Grid-based analysis is identical to that obtained 444
by the EUDPE-UD-based analysis. 445

D. Numerical Results for Coverage Probability

446

We evaluated the coverage probability first by simulation and 447
used the simulated results as the benchmark for the comparison 448
with our theoretical analytic results. We considered two sce- 449
narios. The first case is a single-tier network constructed by 450
macrocells, obeying the uniform random BS distribution and 451
the cellular channel model described in Section II, whereas 452
the second network followed a Poisson BS distribution and 453
obeyed the same cellular channel model of Section II. Given 454
the SINR threshold T , the path-loss exponent α , and the SINR 455
value, the simulated coverage probability was calculated using 456
the pseudocodes presented in Algorithm 1. In the simulation, 457
we set the number of BSs to $N_{\text{BS}} = 80$, the number of UEs to 458
 $N_{\text{UE}} = 10\,000$, the network coverage area to Network Area = 459
 $1000 \times 1000 \text{ m}^2$, and the number of sample simulations to 460
 $N_{\text{max}} = 100$. The average density of BSs was then given as 461

$$\rho = \frac{N_{\text{BS}}}{\text{Network Area}} [\text{BSs/m}^2]. \quad (32)$$

For the Poisson distribution, its intensity was $\lambda = \rho$. We com- 462
pared our low-bound coverage probability results based on the 463
EUDPE-PD and EUDPE-UD models with that of the PPP- 464
based analysis [12]. Since the PPP method can only consider 465
the case of an infinitely large network, we assumed the network 466
boundary $R_{\text{nw}} \rightarrow +\infty$. In the following comparison, the simu- 467
lation results obtained by the network with the uniform random 468
BS distribution are labeled as Simulated data 1, whereas the 469
simulation results yielded by the network with the Poisson BS 470
distribution are denoted Simulated data 2. 471

Algorithm 1 Network Simulation to Evaluate the Coverage Probability.

- 1: Give the number of BSs N_{BS} , the Network Area, and the 472
number of UEs N_{UE} ; 473
- 2: Give the maximum number of sample simulations N_{max} ; 474
- 3: Set Average Coverage Probability = 0; 475
- 4: **for** $N_{\text{sm}} = 1$ to N_{max} **do** 476
- 5: Uniformly and randomly draw the N_{BS} BSs over Net- 477
work Area, or draw the N_{BS} BSs over Network Area by 478
the Poisson distribution; 479

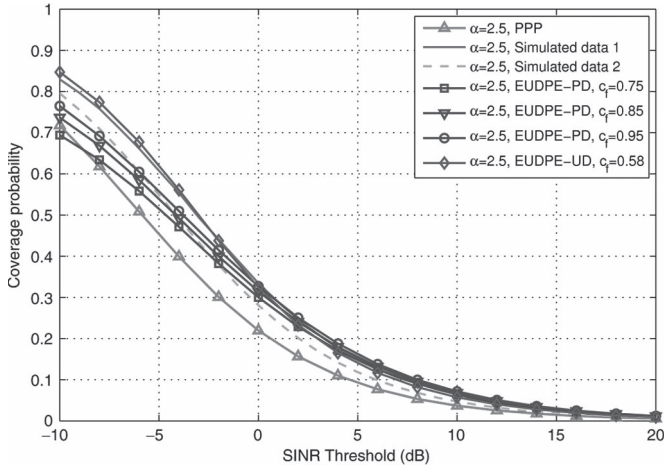


Fig. 7. Comparison of the coverage probabilities based on three different models to the network simulation results, given the path-loss exponent of $\alpha = 2.5$ and no noise, i.e., the AWGN power $\sigma^2 = 0$ and $\text{SINR} = \text{SIR}$.

```

480 6: Uniformly and randomly draw the  $N_{\text{UE}}$  UEs over Net-
481     work Area;
482 7: Initialization: count = 0;
483 8: for  $j = 1$  to  $N_{\text{UE}}$ , do
484 9:     if  $\text{SINR}_j \geq T$  then
485 10:        count = count + 1;
486 11:     end if
487 12: end for
488 13: Coverage Probability = count/ $N_{\text{UE}}$ ;
489 14: Average Coverage Probability +=
490     Coverage Probability;
491 15: end for
492 16: Average Coverage Probability / =  $N_{\text{max}}$ .

```

493 Given the path-loss exponent of $\alpha = 2.5$ and assuming no
494 AWGN or $\sigma^2 = 0$, which implies $\text{SINR} = \text{SIR}$, Fig. 7 shows
495 the coverage probabilities calculated based on the three analytic
496 models, in comparison to the coverage probabilities obtained by
497 the two different network simulations, when varying the SINR
498 threshold. It is shown in Fig. 7 that the coverage probability
499 analysis results of our proposed EUDPE-PD and EUDPE-UD
500 models agree with both simulation results well, better than the
501 PPP-based analysis. When the path-loss exponent is increased
502 to $\alpha = 3$ and 4, the results obtained are shown in Figs. 8
503 and 9, respectively, where it can be seen that the EUDPE-
504 UD analysis agrees with the simulation result based on the
505 network with the uniform random BS distribution better than
506 the other two models, whereas the PPP-based analysis agrees
507 better with the simulation result of the network with the Poisson
508 BS distribution better than the other two models.

509 It is worth emphasizing that because there exist no real
510 network performance data to validate an analysis model, we
511 can only rely on the simulated data. When we have an analysis
512 model agrees with a particular simulation result better than an-
513 other analysis model, it does not imply that the former is better
514 than the latter. The particular simulation result may not actually
515 represent the true real network performance and, moreover, the
516 simulation conditions may not actually match those imposed
517 on an analysis model. What we can claim however is that, if

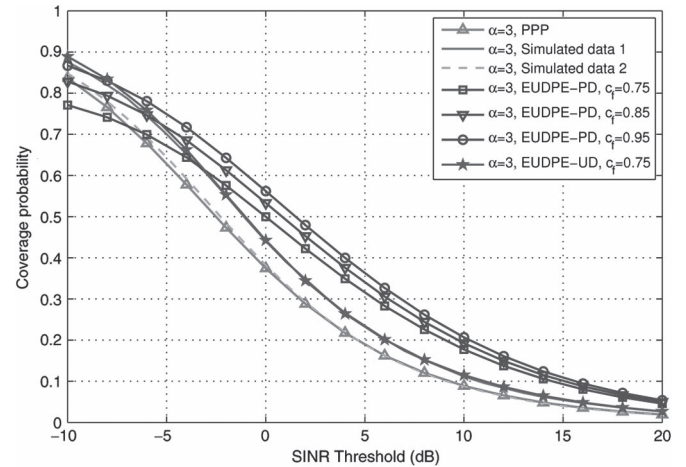


Fig. 8. Comparison of the coverage probabilities based on three different models to the network simulation results, given the path-loss exponent of $\alpha = 3$ and no noise, i.e., the AWGN power $\sigma^2 = 0$ and $\text{SINR} = \text{SIR}$.

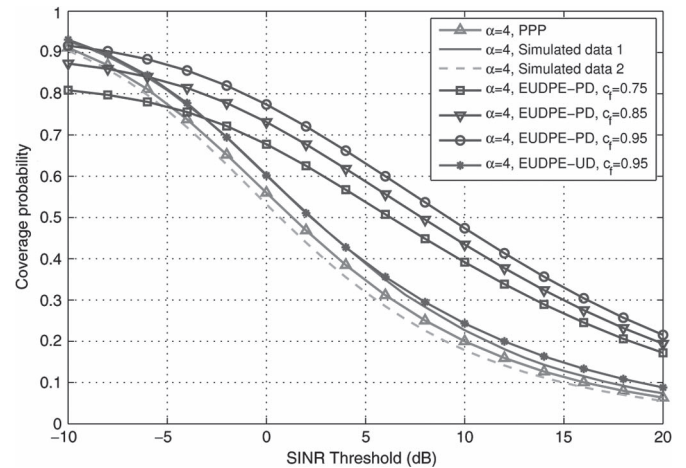


Fig. 9. Comparison of the coverage probabilities based on three different models to the network simulation results, given the path-loss exponent of $\alpha = 4$ and no noise, i.e., the AWGN power $\sigma^2 = 0$ and $\text{SINR} = \text{SIR}$.

an analysis model agrees well with simulation data, it is a rea- 518
519 sonable tool for network analysis and planning. Similarly, if a
520 lower bound coverage probability derived by an analysis model
521 appears to be larger than a simulated coverage probability, it
522 does not imply that this analysis model is wrong. Again, the
523 simulation conditions may not actually match those imposed
524 on the analysis model. For example, we assumed that the
525 network boundary $R_{\text{nw}} \rightarrow +\infty$ for the proposed EUDPE-PD
526 and EUDPE-UD models and the PPP-based analysis for the fair
527 comparison of the three analysis models since the PPP method
528 can only be applied for the case of an infinitely large network.
529 However, the simulated network size was $1000 \times 1000 \text{ m}^2$ and
530 not infinitely large. As shown earlier, another advantage of
531 our analysis approach over the PPP-based method is that our
532 method can be applied to analyze finite-size networks.

533 In our EUDPE-based analysis, the empirical chosen factor
534 c_f is related to the average cell shape and size. The theoretical
535 explanations of this area factor c_f are given in Remark 1.
536 Observe from Fig. 7 that, for the path-loss exponent $\alpha = 2.5$, an
537 appropriate value of this area factor for our EUDPE-UD model
538 is $c_f = 0.58$, which is, in fact, close to the case of the average

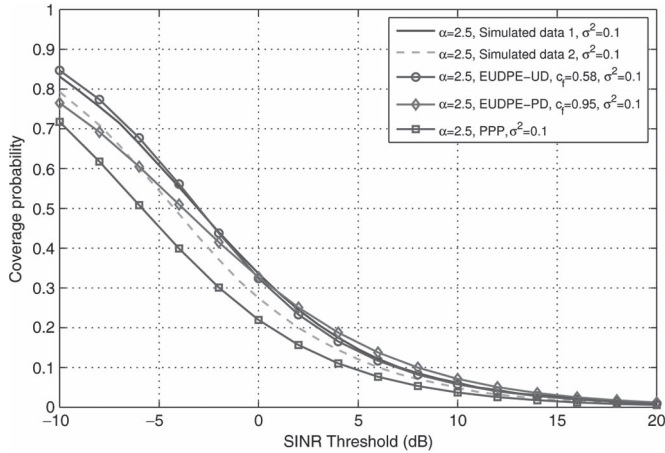


Fig. 10. Comparison of the coverage probabilities based on three different models to the network simulation results, given the path-loss exponent of $\alpha = 2.5$ and the AWGN power $\sigma^2 = 0.1$.

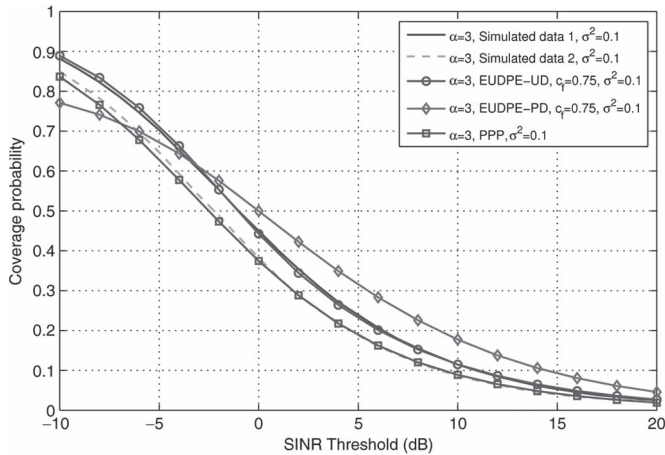


Fig. 11. Comparison of the coverage probabilities based on three different models to the network simulation results, given the path-loss exponent of $\alpha = 3$ and the AWGN power $\sigma^2 = 0.1$.

539 circle-shaped cell. However, as shown in Figs. 8 and 9, as α
 540 increases, the appropriate area factor c_f value also increases. A
 541 plausible explanation for this phenomenon is offered as follows.
 542 As the path-loss exponent α increases, the effective coverage
 543 area R^2/c_f^2 of the serving BS is reduced, and this corresponds
 544 to an increase in the area factor c_f .

545 Next, the effect of noise imposed on the achievable coverage
 546 probability was investigated by setting the AWGN power to
 547 $\sigma^2 = 0.1$ or $10 \log_{10}(1/\sigma^2) = 10$ dB, and the results obtained
 548 are given in Figs. 10–12, respectively, for the three differ-
 549 ent values of α . For graphic clarity, we only draw a single
 550 EUDPE-PD-based coverage probability associated with an ap-
 551 propriate area factor c_f value in each of these three figures.
 552 Again, the same observations as those drawn for Figs. 7–9 can
 553 be made, namely, for the case of $\alpha = 2.5$, the EUDPE-UD-
 554 based analysis agrees with the both simulation results better
 555 than the PPP-based analysis, whereas for higher α values, the
 556 EUDPE-UD analysis matches better with the simulated results
 557 based on the uniform random BS distribution, and the PPP-
 558 based analysis agrees better with the simulated results based

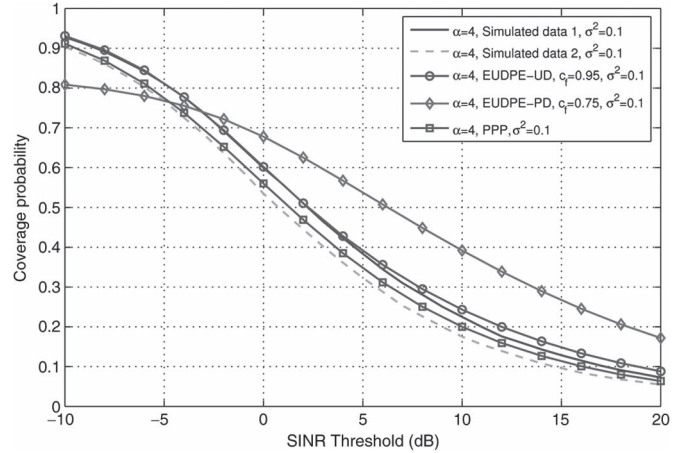


Fig. 12. Comparison of the coverage probabilities based on three different models to the network simulation results, given the path-loss exponent of $\alpha = 4$ and the AWGN power $\sigma^2 = 0.1$.

on the Poisson BS distribution. Upon comparing Figs. 10–12
 with Figs. 7–9, it can be seen that the effect of the channel
 AWGN to the achievable coverage probability is minor. For
 example, observe that the simulated-data-2 curve in Fig. 7
 almost matches the simulated-data-2 curve in Fig. 10, whereas
 the PPP-analysis-based curve in Fig. 7 is almost identical to the
 PPP-analysis-based curve in Fig. 10. Similarly, the other three
 coverage probability curves in Fig. 10 also closely match the
 corresponding coverage probability curves in Fig. 7.

V. AVERAGE ACHIEVABLE RATE ANALYSIS USING EQUIVALENT UNIFORM DENSITY PLANE-ENTITY

Let us now apply the proposed EUDPE method to analyze
 the average achievable throughput. According to Shannon's
 theory, under the idealized simplifying condition of having a
 Gaussian interference owing to the central limit theorem, the
 average achievable rate is defined as [12]

$$C \triangleq \mathbb{E}[\ln(1 + \text{SINR})]. \quad (33)$$

Since we are concerned with the system's achievable through-
 put, we will consider the case of the network boundary being
 sufficiently far away, i.e., $R_{\text{nw}} \rightarrow +\infty$.

A. Average Achievable Rate Analysis Using EUDPE-PD

Again, we first consider the case that the geographic BS
 distribution follows a Poisson distribution, and we have the
 following result.

Theorem 5: For the network where the BS geographic
 distribution obeys the Poisson distribution of intensity λ , a
 lower bound for the average achievable throughput is given by

$$C_l(\lambda, \alpha) = \pi \lambda \int_0^{R^2} e^{-\pi \lambda v} \left(\int_{t>0} e^{-\bar{h} v \alpha / 2 (e^t - 1) \chi(\alpha, v)} dt \right) dv \quad (34)$$

where $\chi(\alpha, v)$ is given in (25).

586 *Proof:* According to [12], we have

$$C(\lambda, \alpha) = \int_0^R 2\pi\lambda r e^{-\pi\lambda r^2} \times \int_{t>0} \mathbb{E}_{I_r} [\mathbb{P}\{h_0 > P^{-1}r^\alpha(e^t - 1)(\sigma^2 + I_r)\}] dt dr. \quad (35)$$

587 Similar to Corollary 2, we have

$$\mathbb{E}_{I_r} [\mathbb{P}\{h_0 > P^{-1}r^\alpha(e^t - 1)(\sigma^2 + I_r)\}] \geq e^{-\bar{h}r^\alpha(e^t - 1)\xi(\alpha, r)} \quad (36)$$

588 where $\xi(\alpha, r)$ is defined in (20). Thus, a lower bound of $C(\lambda, \alpha)$
589 is given by

$$C_l(\lambda, \alpha) = \int_0^R 2\pi\lambda r e^{-\pi\lambda r^2} \left(\int_{t>0} e^{-\bar{h}r^\alpha(e^t - 1)\xi(\alpha, r)} dt \right) dr. \quad (37)$$

590 By defining $v = r^2$ in (37), we obtain (34). ■

591 *Corollary 5:* In the noise-free case, namely, $\sigma^2 = 0$, a lower
592 bound for the average achievable throughput is

$$C_l(\lambda, \alpha) = \pi\lambda \int_0^{R^2} e^{-\pi\lambda v} \left(\int_{t>0} e^{-\bar{h}v^{\alpha/2}(e^t - 1)\bar{\chi}(\alpha, v)} dt \right) dv \quad (38)$$

593 where

$$\bar{\chi}(\alpha, v) = \frac{2\pi\rho\bar{h}}{\alpha - 2} (2R - v^{1/2})^{2-\alpha}. \quad (39)$$

594 B. Average Achievable Rate Analysis Using EUDPE-UD

595 Next, we consider the case that the geographic BS distribu-
596 tion follows a uniform random distribution, and we have the
597 following result.

598 *Theorem 6:* For the network where the BS geographic dis-
599 tribution obeys the uniform random distribution with an average
600 BS density of ρ , a lower bound for the average achievable
601 throughput is given by

$$C_l(\rho, \alpha) = \frac{\rho}{c_f^2} \int_0^{R^2} \left(\int_{t>0} e^{-\bar{h}v^{\alpha/2}(e^t - 1)\chi(\alpha, v)} dt \right) dv \quad (40)$$

602 where $\chi(\alpha, v)$ is given in (25).

603 *Proof:* Noting that the average achievable throughput is
604 defined as

$$C(\lambda, \alpha) = \frac{\rho}{c_f^2} \int_0^R 2r \times \int_{t>0} \mathbb{E}_{I_r} [\mathbb{P}\{h_0 > P^{-1}r^\alpha(e^t - 1)(\sigma^2 + I_r)\}] dt dr \quad (41)$$

605 the proofs are similar to the proofs for Theorem 5. ■

Corollary 6: In the noise-free case, namely, $\sigma^2 = 0$, a lower
606 bound for the average achievable throughput is 607

$$C_l(\rho, \alpha) = \frac{\rho}{c_f^2} \int_0^{R^2} \left(\int_{t>0} e^{-\bar{h}v^{\alpha/2}(e^t - 1)\bar{\chi}(\alpha, v)} dt \right) dv. \quad (42)$$

608 where $\bar{\chi}(\alpha, v)$ is given in (39).

Remark 3: It is straightforward to carry out the average
609 achievable throughput analysis for any deterministic grid-based
610 cellular network model, because the EUDPE-Grid model is a
611 special case of the EUDPE-UD model. Therefore, the lower
612 bound of the average achievable throughput for the grid-based
613 network model is also given in Theorem 6. Moreover, under the
614 equivalent network environment of the same ρ and R values,
615 the lower bound of the average achievable throughput obtained
616 by the EUDPE-Grid-based analysis is identical to that obtained
617 by the EUDPE-UD-based analysis. 618

619 C. Numerical Results for Average Achievable Rate

Assuming a unity frequency reuse factor, we compare the
620 lower bounds of the average achievable throughput obtained
621 by the proposed EUDPE-PD- and EUDPE-UD-based analyses
622 to that of the PPP-based analysis [12] in Fig. 13 by varying
623 the path-loss exponent value. The simulated average achiev-
624 able throughputs obtained from the two network simulations
625 with the uniform random BS distribution and the Poisson BS
626 distribution are labeled as Simulated rate 1 and Simulated
627 rate 2, respectively, and they are also given in Fig. 13 as the
628 benchmark. For our proposed EUDPE-PD and EUDPE-UD-
629 based analysis and the network simulations, both the noise-
630 free and noisy results are presented. However, for the
631 PPP-based average achievable throughput analysis, only the
632 noise-free case is provided in [12]; therefore, in Fig. 13, we only
633 present the noise-free PPP-based result. It can be observed that
634 all the three theoretical analysis based results and the simulation
635 data all reveal that the average achievable throughput increases
636 linearly, as the path-loss exponent increases. More specifically,
637 all the analytical and simulated data have accurate linear fitting.
638 It is also shown in Fig. 13 that our proposed EUDPE-PD-
639 and EUDPE-UD-based analyses agree with the two simulated
640 results better than the PPP-based analysis, particularly for the
641 path-loss exponent $\alpha \leq 4.5$. The results of Fig. 13 also show
642 that the noise only has a minor effect on the average achievable
643 throughput, which is expected as we consider the interference-
644 limited scenario with a unity frequency reuse factor. 645

646 VI. CONCLUSION

We have proposed a universal approach for accurately
647 analyzing the coverage probability and average achievable
648 throughput of cellular networks. More specifically, we have
649 derived a generic EUDPE procedure for evaluating the other-
650 cell interference. Based on this EUDPE interference model, we
651 have derived the lower bounds of both the coverage probability
652 and average achievable throughput for various practical BS
653 distribution models, including the stochastic Poisson distributed
654 model, uniformly and randomly distributed model, and the 655

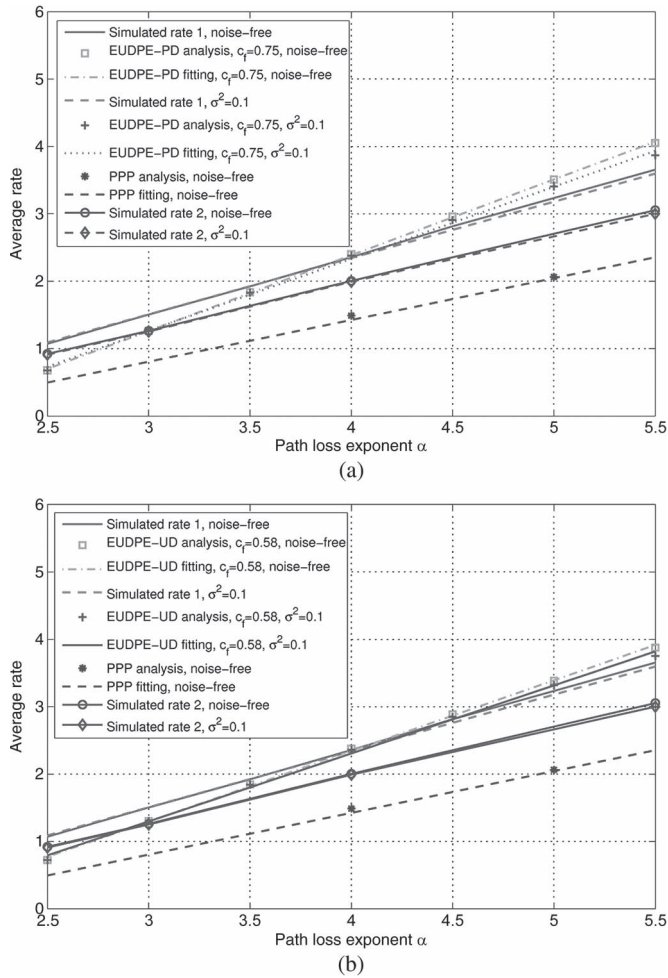


Fig. 13. Comparison of the average achievable throughputs based on three different models to the network simulation results, given different path-loss exponent values. (a) EUDPE-PD and PPP models and (b) EUDPE-UD and PPP models.

deterministic grid-based model. Extensive simulation results have validated that the coverage probability and average throughput obtained by our proposed universal analysis method agree with the simulated coverage probability and average throughput at least as closely as those obtained by the popular existing PPP-based analysis, if not better. In addition, we have also introduced a generic and physical definition of cell edge boundary. We have shown that the popular hexagonal and Voronoi network topologies only emerge from the grid-based network model and the random BS distribution model, respectively, given an unrealistic high path-loss exponent according to this definition. Moreover, we have demonstrated that the cell edge boundary shows irregular near-circular shapes, given a more realistic path-loss exponent, which cannot be modeled accurately by either hexagonal or Voronoi topology.

REFERENCES

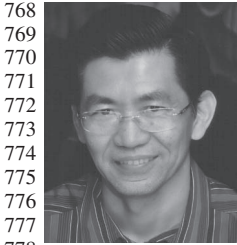
[1] A. Damnjanovic *et al.*, "A survey on 3GPP heterogeneous networks," *IEEE Wireless Commun.*, vol. 18, no. 3, pp. 10–21, Jun. 2011.
 [2] J. G. Andrews, "Seven ways that hetnets are a cellular paradigm shift," *IEEE Commun. Mag.*, vol. 51, no. 3, pp. 136–144, Mar. 2013.
 [3] A. Ghosh, *et al.*, "Heterogeneous cellular networks: From theory to practice," *IEEE Commun. Mag.*, vol. 50, no. 6, pp. 54–64, Jun. 2012.

[4] J. G. Andrews, H. Claussen, M. Dohler, S. Rangan, and M. C. Reed, "Femtocells: Past, present, and future," *IEEE J. Sel. Areas Commun.*, vol. 30, no. 3, pp. 497–508, Apr. 2012.
 [5] X. Yang and A. P. Petropulu, "Co-channel interference modeling and analysis in a Poisson field of interferers in wireless communications," *IEEE Trans. Signal Process.*, vol. 51, no. 1, pp. 64–76, Jan. 2003.
 [6] A. D. Wyner, "Shannon-theoretic approach to a Gaussian cellular multiple-access channel," *IEEE Trans. Inf. Theory*, vol. 40, no. 6, pp. 1713–1727, Nov. 1994.
 [7] S. Shamai and A. D. Wyner, "Information-theoretic considerations for symmetric, cellular, multiple-access fading channels, Part I," *IEEE Trans. Inf. Theory*, vol. 43, no. 6, pp. 1877–1894, Nov. 1997.
 [8] S. Shamai and A. D. Wyner, "Information-theoretic considerations for symmetric, cellular, multiple-access fading channels, Part II," *IEEE Trans. Inf. Theory*, vol. 43, no. 6, pp. 1895–1911, Nov. 1997.
 [9] J. Xu, J. Zhang, and J. G. Andrews, "On the accuracy of the Wyner model in cellular networks," *IEEE Trans. Wireless Commun.*, vol. 10, no. 9, pp. 3098–3109, Sep. 2011.
 [10] F. Baccelli, M. Klein, M. Lebourges, and S. Zuyev, "Stochastic geometry and architecture of communication networks," *Telecommun. Syst.*, vol. 7, no. 1–3, pp. 209–227, Jun. 1997.
 [11] T. X. Brown, "Cellular performance bounds via shotgun cellular systems," *IEEE J. Sel. Areas Commun.*, vol. 18, no. 11, pp. 2443–2455, Nov. 2000.
 [12] J. G. Andrews, F. Baccelli, and R. K. Ganti, "A tractable approach to coverage and rate in cellular networks," *IEEE Trans. Commun.*, vol. 59, no. 11, pp. 3122–3134, Nov. 2011.
 [13] R. W. Heath and M. Kountouris, "Modeling heterogeneous network interference," in *Proc. IEEE ITA*, San Diego, CA, USA, Feb. 5–10, 2012.
 [14] H. S. Dhillon, R. K. Ganti, F. Baccelli, and J. G. Andrews, "Modeling and analysis of K-tier downlink heterogeneous cellular networks," *IEEE J. Sel. Areas Commun.*, vol. 30, no. 3, pp. 550–560, Apr. 2012.
 [15] M. Z. Win, P. C. Pinto, and L. A. Shepp, "A mathematical theory of network interference and its applications," *Proc. IEEE*, vol. 97, no. 2, pp. 205–230, Feb. 2009.
 [16] A. Busson and G. Chelius, "Point processes for interference modeling in CSMA/CA ad-hoc networks," in *Proc. 6th ACM Symp. Performance Eval. Wireless Ad Hoc, Sens., Ubiquitous Netw.*, Tenerife, Canary Islands, Spain, Oct. 26–30, 2009.
 [17] F. Baccelli, B. Błaszczyszyn, and P. Mühlethaler, "An Aloha protocol for multihop mobile wireless networks," *IEEE Trans. Inf. Theory*, vol. 52, no. 2, pp. 421–436, Feb. 2006.
 [18] H. Q. Nguyen, F. Baccelli, and D. Kofman, "A stochastic geometry analysis of dense IEEE 802.11 networks," in *Proc. 26th IEEE INFOCOM*, Anchorage, AK, USA, May 6–12, 2007.
 [19] M. L. Huber and R. L. Wolpert, "Likelihood-based inference for Matérn type-III repulsive point processes," *Adv. Appl. Probab.*, vol. 41, no. 4, pp. 958–977, Dec. 2009.
 [20] M. Haenggi, "Mean interference in hard-core wireless networks," *IEEE Commun. Lett.*, vol. 15, no. 8, pp. 792–794, Aug. 2011.
 [21] A. Hasan and J. G. Andrews, "The guard zone in wireless ad hoc networks," *IEEE Trans. Wireless Commun.*, vol. 6, no. 3, pp. 897–906, Mar. 2007.
 [22] B. Cho, K. Koufos, and R. Jantti, "Bounding the mean interference in Matérn type II hard-core wireless networks," *IEEE Wireless Commun. Lett.*, vol. 2, no. 5, pp. 563–566, Oct. 2013.
 [23] F. Jarai-Szabo and Z. Neda, "On the size-distribution of Poisson Voronoi cells," *Phys. A, Statist. Mech. Appl.*, vol. 385, no. 2, pp. 518–526, Feb. 2007.
 [24] D. Cao, S. Zhou, and Z. Niu, "Optimal combination of base station densities for energy-efficient two-tier heterogeneous cellular networks," *IEEE Trans. Wireless Commun.*, vol. 12, no. 9, pp. 4350–4362, Sep. 2013.
 [25] S. Lee and K. Huang, "Coverage and economy of cellular networks with many base stations," *IEEE Commun. Lett.*, vol. 16, no. 7, pp. 1038–1040, Jul. 2012.
 [26] J.-M. Kelif, M. Coupechoux, and P. Godlewski, "A fluid model for performance analysis in cellular networks," *EURASIP J. Wireless Commun. Netw.*, vol. 2010, pp. 1–11, Aug. 2010.
 [27] F. Baccelli and B. Błaszczyszyn, *Stochastic Geometry and Wireless Networks, Volume I: Theory*. Hanover, MA, USA: Now, 2009.
 [28] M. Haenggi, *Stochastic Geometry for Wireless Networks*. Cambridge, U.K.: Cambridge Univ. Press, 2013.
 [29] M. Kuczma, *An Introduction to the Theory of Functional Equations and Inequalities: Cauchy's Equation and Jensen's Inequality*. Basel, Switzerland: Birkhauser, 2008.



Hui Zhang received the B.Eng. degree in applied mathematics and the Ph.D. degree in electrical engineering from Beijing University of Posts and Telecommunications, Beijing, China, in 2005 and 2010, respectively.

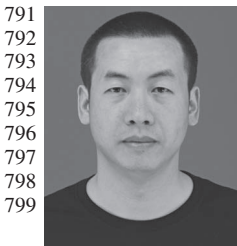
Since 2010, he has been a faculty member with the School of Electrical Information and Optical Engineering, Nankai University, Nankai, China. From 2013 to 2014, he was a Postdoctoral Scholar with the School of Electrical and Computer Science, University of Southampton, Southampton, U.K. In 2014, he joined in the China–Korea Young Scientist Exchange Program. His research interests include cellular networks and wireless communication theory.



Sheng Chen (M'90–SM'97–F'08) received the B.Eng. degree in control engineering from the East China Petroleum Institute, Dongying, China, in 1982; the Ph.D. degree in control engineering from the City University London, London, U.K., in 1986; and the D.Sc. degree from the University of Southampton, Southampton, U.K., in 2005.

From 1986 to 1999, he held research and academic appointments with The University of Sheffield, Sheffield, U.K.; The University of Edinburgh, Edinburgh, U.K.; and the University of Portsmouth, Portsmouth, U.K. Since 1999, he has been with Electronics and Computer Science, the University of Southampton, Southampton, U.K., where he is currently a Professor of intelligent systems and signal processing. He is also a Distinguished Adjunct Professor with King Abdulaziz University, Jeddah, Saudi Arabia. He is the author of over 500 research papers. His research interests include adaptive signal processing, wireless communications, modeling and identification of nonlinear systems, neural network and machine learning, intelligent control system design, and evolutionary computation methods and optimization.

779 Dr. Chen is a Fellow of the Institution of Engineering and Technology and
780 an ISI highly cited researcher in engineering (March 2004). In 2014, he was
781 elected as a Fellow of the United Kingdom Royal Academy of Engineering.



Liang Feng received the B.Eng. degree in applied physics from Dalian University of Technology, Dalian, China, in 2004. He is currently working toward the Master's degree with Nankai University, Nankai, China, in 2012.

From 2004 to 2012, he carried out electronic countermeasures research with the Luoyang Electronic Equipment Center, China. His research interests include cellular mobile communications.



Yifeng Xie received the B.S. degree in electronic and information engineering from Nanjing Forestry University, Nanjing, China, in 2011 and the M.S. degree in communication and information systems from Nankai University, Nankai, China, in 2014.

His research interests include stochastic geometry and heterogeneous networks.



Lajos Hanzo (F'08) received the Master's and D.Sc. degrees in electronics and the Doctor Honoris Causa from the Technical University of Budapest, Budapest, Hungary, in 1976 and 1983, respectively.

During his 38-year career in telecommunications, he has held various research and academic posts in Hungary, Germany, and the U.K. Since 1986, he has been with the School of Electronics and Computer Science, University of Southampton, Southampton, U.K., where he is the Chair in telecommunications.

He has successfully supervised about 100 Ph.D. students. He is the author or coauthor of 20 John Wiley/IEEE Press books on mobile radio communications, totalling in excess of 10 000 pages, and of more than 1400 research entries on IEEE Xplore. Currently, he is directing a 100-strong academic research team, working on a range of research projects in the field of wireless multimedia communications sponsored by industry, the Engineering and Physical Sciences Research Council (EPSRC) U.K., the European Research Council's Advanced Fellow Grant, and the Royal Society's Wolfson Research Merit Award. He is an enthusiastic supporter of industrial and academic liaison, and he offers a range of industrial courses.

Dr. Hanzo has acted both as a Technical Program Committee Chair and as a General Chair of IEEE conferences, has presented keynote lectures, and has received a number of distinctions. He is a Governor of the IEEE Vehicular Technology Society. From 2008 to 2012, he was the Editor-in-Chief of the IEEE Press and a Chaired Professor with Tsinghua University, Beijing, China. His research is funded by the European Research Council's Senior Research Fellow Grant. He is a Fellow of the Royal Academy of Engineering, the Institution of Engineering and Technology, and the European Association for Research and Signal Processing.

AUTHOR QUERIES

AUTHOR PLEASE ANSWER ALL QUERIES

AQ1 = Note that Ref. [7] was split into two. Consequently, the reference list and bibliographic citations were renumbered. Please check.

END OF ALL QUERIES